Numerical Investigation of Copper-Water Nanofluid in a Parallel Plate Channel

Saeb Ragani Lamooki

Submitted to the
Institute of Graduate Studies and Research
in partial fulfillment of the requirements for the Degree of

Master of Science
in
Mechanical Engineering

Eastern Mediterranean University
June 2014
Gazimagusa, North Cyprus

Approval of the Institute of Graduate Studies and Research

_____
Prof. Dr. Elvan Yılmaz
Director

I certify that this thesis satisfies the requirements as a thesis for the degree of Master of Science in Mechanical Engineering.

_____
Prof. Dr. Uğur Atikol
Chair, Department of Mechanical Engineering

We certify that we have read this thesis and that in our opinion it is fully adequate in scope and quality as a thesis for the degree of Master of Science in Mechanical Engineering.

_____
Prof. Dr. İbrahim Sezai
Supervisor

Examining Committee
_____

1. Prof. Dr. Fuat Egelioğlu   _____

2. Prof. Dr. İbrahim Sezai   _____

3. Assoc. Prof. Dr. Hasan Hacışevki   _____

ABSTRACT

Heat transfer behavior of Cu-water nanofluid in a two dimensional (infinite depth) rectangular duct is studied numerically for laminar flow, where the nanofluid has been considered as a Newtonian fluid. The governing continuity, momentum, and energy equations are discretized using finite volume approach and solved using SIMPLE method. The viscosity and thermal conductivity of nanofluid are determined by models proposed by Brinkman and Patel et al. Study has been conducted for a wide range of Reynolds number from 10 to 1500, for solid volume fractions between 0% and 5%. Top and bottom walls are considered for two cases of constant temperature and constant wall heat flux, while results for both uniform and parabolic entrance velocities are considered in each case. It has been observed that the rate of heat transfer increases with increase in solid volume fraction as well as increase in flow rate. Besides, higher heat transfer is observed for uniform entrance velocity compared to channel with parabolic inlet velocity.

Keywords: Nanofluid, Rectangular duct, Laminar flow, Newtonian

ÖZ

Bakır-Su nano-sıvısının ısı transferi davranış ve iki boyutlu dikdörtgen kanal içerisinde sayısal ve nümerik olarak laminer akım için gözlemlenip incelenmiştir. Burada nano-sıvı bir Newton sıvısı olarak düşünülmüştür. Akımın sürekliliği ve istikrarı, ivme ve enerji eşitlikleri sonlu elemanlar yöntem ve analizi kullanılarak ayrıştırılmıştır ve "Simple" yöntemi kullanılarak çözümlendirilmiştir. Nano-sıvının akışkanlığı ve termal iletkenliği Brinkman ve Patel modelleri ile belirlenmiştir. Çalışma 10 Reynolds sayısından 1500 Reynolds sayısına kadar olmak üzere çok geniş Reynolds sayısı aralığında %0 dan %5'e kadar olan katı hacim yüzdeleri için yapılıp sürdürülmüştür. Alt ve üst duvarlar sabit sıcaklıkta ve sabit duvar ısı akışında olmak üzere iki farklı durumda düşünülüp incelenirken hem düzgün hem de parabolik giriş hızları sonuçları her iki durumda da ayrı ayrı incelenmiştir. Sıvı içindeki katı hacim yüzdesi arttıkça ısı transferinin yükseldiği görülmüştür. Bunun yanında düzgün hız girişli akışın, parbolik hız girişli akıştan daha yüksek ısı transferi sağladığı gözlemlenmiştir.

Anahtar kelimeler: nano-sıvısı, dikdörtgen kanal, laminer akım, Newton sıvısı

ACKNOWLEDGEMENT

It was impossible for me to finish my dissertation without the help of my supervisor.

I would like to express my sincerest gratitude to Professor Dr. Ibrahim Sezai for his great help and support.

I would also like to thank my family, which has always supported me and encouraged me with best wishes.

TABLE OF CONTENTS

LIST OF TABLES

LIST OF FIGURES

LIST OF SYMBOLS

t Time, [s]

$\vec{V}$ Velocity vector, $[m/s]$

u Velocity component in x direction, $[m/s]$

v Velocity component in y direction, $[m/s]$

P Pressure, $[Pa]$

x Horizontal coordinate, $[m]$

y Vertical coordinate, $[m]$

T Temperature, $[K]$

C_p Specific heat, $[J/kg\ K]$

k Thermal conductivity, $[W/m\ K]$

c Empirical constant, $c = 3.60 \times 10^4$

Pe Peclet number

d_p Solid particles diameter, $[m]$

d_f Molecular size of the base fluid, $2\ \text{Å}$

u_p Brownian motion velocity of the particles, $[m/s]$

K_b Boltzmann constant, $[J/K]$

L_{ref} Reference length, $[m]$

L Channel length, $[m]$

H Channel width, $[m]$

Nu_x Local wall Nusselt number, $Nu = \dfrac{h\ L_{ref}}{k_f}$

$\overline{Nu}$ Average wall Nusselt number, $\overline{Nu} = \dfrac{1}{L}\int_0^L Nu_x\ dx$

T_b Flow bulk temperature, $[K]$

A_c Channel cross section area, $[m^2]$

q_w Wall heat flux, $[W/m^2]$

Re Reynolds number, $Re = \dfrac{\rho_f\, U_{ref}\, H}{\mu_f}$

Pr Prandtl number, $Pr = \dfrac{\mu_f C_{p_f}}{k_f}$

U_m Mean inlet velocity, $[m/s]$

D_e Equivalent diameter, $[m]$

A_f Flow area, $[m^2]$

P Cross section perimeter, $[m]$

$\dot{m}$ Mass flow rate, $[kg/s]$

Greek Symbols

ρ Density, $[kg/m^3]$

α Thermal diffusivity, $[m^2/s]$

ϕ Nanoparticle volume fraction

μ_f Dynamic viscosity, $[Ns/m^2]$

τ_x Wall local shear stress, $[N/m^2]$

$\bar{\tau}$ Wall average shear stress, $[N/m^2]$

Subscript

eff   Effective

f   Base fluid

p   Nanoparticle

nf   Nanofluid

ref   Reference

w	Wall
in	Inlet
out	Outlet
b	bulk
m	mean

Chapter 1

INTRODUCTION

1.1 Introduction to Nanofluids

Vast range of industrial processes deals with the transfer of heat energy. In almost all industrial equipments heat should be added, removed or transferred from one part to another and this is a prominent task in industry.

Higher efficiency in heating and cooling saves energy and time and increases the lifetime of the equipments. Some processes are even affected qualitatively by higher efficiency of heat transfer. Nowadays systems with higher heat transfer efficiencies are popular. Some works have been done for better understanding of heat transfer and it's augmentation in practical applications. The emerge of processes with high heat have increased the demand for modern technologies in heat transfer. There are several methods to increase the heat transfer rate. Some are based upon the increment of heat transfer surface, vibrating the heat transfer surface, and using microchannels. Moreover, heat transfer increases with an increase in thermal conductivity of the working fluid. Common working fluids in heat transfer industry such as water, ethylene glycol, and engine oil have low thermal conductivities compared to solids. For example, thermal conductivity of copper is 670 times greater than thermal conductivity of water at 25℃ and in the case of multi-wall carbon nanotubes (MWCNTs) at room temperature it is 20000 times greater than engine oil. The high conductivity of solids can be utilized to increase the conductivity of fluids by adding

small solid particles to fluid so that the new suspension has greater conductivity compared to pure fluid. The possibility of using suspensions with the size of solid particles in the range of 2 millimeters or micrometers has been observed by some researchers in the past and following drawbacks have been reported (S. K. Das, Choi, & Patel, 2006):

1. The bigger the size of solid particles, higher is the chance of sedimentation. When solid particles settle on the surface of their container, heat transfer decreases.

2. High velocity of solid particle-fluid suspensions over a surface decreases the rate of sedimentation but increases the chance of surface erosion.

3. Clogging is another disadvantage of these suspensions especially in the case of narrow passages and microchannels.

4. Pressure drop increases considerably compared to the case of pure fluid.

5. Eventually the increment of thermal conductivity with the enhancement of solid particle concentration (i.e., increasing particle concentration causes higher thermal conductivity of the suspension and subsequently increasing the abovementioned problems).

The problems related to microscale particle-fluid suspensions have become significantly less intense after new material technologies made it possible to produce nanoscale particles, which are quite different from the parent material in mechanical, thermal, electrical, and optical properties.

A properly dispersed nanofluid suspension has the following advantages compared to the conventional micro-sized particle-fluid suspensions (S. K. Das et al., 2006):

1. Increased conduction heat transfer as a result of increased surface area of the particles. Particles with diameters less than 20 nm carry 20% of their atoms on their surface make them better medium for heat transfer. Besides the small size of these particles let them move faster in the suspension which brings about micro-convection of fluid and hence increased heat transfer. This micro-convection in turn speeds up the dispersion of heat in the fluid. This is the main reason for increase in thermal conductivity of nanofluid by an increase in temperature.

2. Because of the small weight of particles the chances of sedimentation are less so the Brownian motion dominates their weight and as a result of that the suspension will be more stable.

3. Using micro-particles in microchannels always have the problem of clogging. The nanofluid overcomes this problem as it contains finer particles.

4. The small nanoparticles impart smaller momentum to solid walls of equipments such as exchangers, pipes, and pumps.

5. In conventional fluids to increase the heat transfer by a factor of two it is needed to increase the pumping power by a factor of ten. On the other hand in the same apparatus heat transfer can be doubled if thermal conduction is tripled (Choi & Eastman, 1995). Thus pumping power can be saved considerably as a result of

thermal conductivity increase in nanofluid as far as there is not a sharp increase in nanofluid's viscosity.

Nanoparticles can be mainly divided into three categories: ceramic particles, pure metallic particles, and carbon nanotubes (CNTs) and some of the base fluids have been used so far include water, ethylene glycol, transformer oil, and toluene.

Models initially proposed for prediction of effective thermal conductivity of nanofluids (e.g. Maxwell-Garnett model (Garnett, 1904) and Hamilton-Crosser model (Hamilton & Crosser, 1962)) mainly included thermal conductivity of base fluid and particles, solid volume fraction of particles, and the shape of nanoparticles. Further experiments to measure nanofluids thermal conductivity proved an important dependence on nanoparticle size and temperature. Even small temperature change which does not affect the thermal conductivity of base fluid and nanoparticle, has a considerable effect on nanofluid thermal conductivity. This fact indicated that some kind of particle movement that dramatically changes with temperature must be taking place within the fluid.

While applying nanofluids for commercial cooling Tzeng et al. (Tzeng, Lin, & Huang, 2005) investigated the performance of both $CuO(4.4\%$ wt$)$ and $Al_2O_3(4.4\%$ wt$)$ nanoparticles dispersed in automatic transmission oil as engine coolant. Comparing the results with conventional antifoam-oil coolant indicated that CuO nanofluid had the best heat transfer effect and antifoam-oil showed the worst effect.

1.2 Objective of Thesis

The effect of copper particle volume fraction on heat transfer rate of copper-water nanofluid flow in a parallel plate channel is investigated in this work. Local and

average Nusselt numbers have been calculated numerically to measure the heat transfer rate of the flow.

Moreover, four different boundary conditions have been considered in the work as following:

1- Constant Wall Temperature and Uniform Entrance Velocity

2- Constant Wall Temperature and Parabolic Entrance Velocity

3- Constant Wall Heat Flux and Uniform Entrance Velocity

4- Constant Wall Heat Flux and Parabolic Entrance Velocity

Local and average Nusselt numbers have been calculated for all cases to find the effect of abovementioned boundary conditions on heat transfer rate of the channel.

1.3 Overview of Thesis Work

In chapter one an introduction to nanofluid and its history is briefly presented.

In chapter two a review over the related literature has been done and the models for nanofluid thermophysical properties are discussed to choose the best models among existing ones.

In chapter three the governing equations for the problem are presented. Models, relations, and the problem boundary conditions are discussed thoroughly in this

chapter. An explanation about the numerical approach is presented at the end of this chapter.

In chapter four results in the form of graphs and tables are presented and discussed.

In chapter five conclusions and remarks about the final results are reported.

Chapter 2

LITERATURE SURVEY

Nanofluid is a mixture of a base fluid and small nano-sized solid particles. The size of nanoparticles is usually in the range of 1 to 100nm and the volume fraction of particles is normally below 5-10%. There are several kinds of base fluids and nanoparticles used to form these nanofluids, e.g. water, ethylene glycol, Propylene or oil as base fluid and copper, copper oxide, aluminum oxide or carbon nanotubes as nanoparticle. The most important feature of these mixtures is their improved thermal conductivity which depends upon factors such as the shape of particles, the dimension of particles, the volume fraction of particles, and thermal properties of particle materials. Xuan et al. (Xuan and Roetzel, 2000) have examined the transport properties of nanofluid and have expressed that thermal dispersion, which takes place due to the random movements of particles, takes a major role in increasing the heat transfer rate between the fluid and the wall. Brownian motion of the particles, ballistic phonon transport through the particles and nanoparticle clustering can also be the possible reasons for this enhancement. At small length scales, the classical diffusion-based model for heat conduction begins to fail. This makes modeling the energy transport challenging. In semiconductors and insulators, heat is carried primarily by vibrations in the crystal lattice known as phonons. Das et al. (Das et al., 2003) has observed that the thermal conductivity for nanofluids increases with increasing temperature.

Convective heat transfer plays an important role in a variety of thermal systems such as power plants, refrigerators, and small electronic devices. Using nanofluids in such equipments are helpful to increase the performance of cooling systems as well as reducing their size. Emerge of nanofluids opened a new way in heat transfer industry that can be the most impressive recent innovation in thermal science.

The idea of using solid-liquid mixtures is not a new idea, but in conventional mixtures millimeter or micrometer-sized particles were used, which had the disadvantages of clogging, erosion, sedimentation, and severe pressure drop. Recent advancements in material technology, during last decades has made it possible to make nano-size particles which can be used in solid liquid mixtures with an advantage of improved thermal properties and very small or none of the problems of conventional mixtures.

There are several correlations for thermal conductivity of nanofluids in literature. The models proposed by Hamilton and Crosser (Hamilton & Crosser, 1962), Wasp (Wasp, Kenny, & Gandhi, 1977), Maxwell-Garnett (Garnett, 1904), Bruggeman (Bruggeman, 1935), and Wang et al. (B. X. Wang, Zhou, & Peng, 2003) failed to predict thermal conductivity of nanofluids accurately. The experimental results show a much higher thermal conductivity of nanofluid than those predicted by abovementioned models. Jang and Choi's model (Jang & Choi, 2004) is a Brownian motion induced model which accounts for the effects of nanoparticle's concentration, size and temperature. Kumar et al. (Kumar et al., 2004) has proposed a model where effective thermal conductivity is a function of both temperature and particle diameter. Patel et al. (Patel et al., 2005) has improved the Kumar et al.'s model by incorporating the effect of microconvection due to particle movement. Since the

8

Brownian motion rises with temperature, the temperature effect is considered which results in higher convection. This model is applicable to low concentration of solid particles. Moreover, this model considers the effect of the size of nanoparticle through an increase in specific surface of nanoparticles (S. Das, Sundararajan, Pradeep, & Patel, 2005). Likewise, an empirical constant 'c', links the temperature dependence of effective thermal conductivity to the Brownian motion of the particles. This constant (c) can be found by comparing the calculated value with experimental data, which comes in the order of 10^4. This empirical constant is adjustable and can be thought as a function of particle properties as well as size (Patel et al., 2005).

The same problem exists for effective viscosity of nanofluid. Comparing different correlations for nanofluids effective viscosity with experimental values from previous investigations on Al_2O_3 nanofluids by Lee et al. (J.H. Lee, 2005) and Wang et al. (X. Wang, Xu, & S. Choi, 1999) do not show good agreement. Einstein's model (Einstein, 1956) Brinkman's model (Brinkman, 1952), and Brownian motion effect's model underestimates effective viscosity of water based Al_2O_3 nanofluid compared to mentioned experimental results, while Pak and Cho's correlation overestimates it in volume fractions more than 0.1 % (Hwang, Lee, & Jang, 2007). Based upon this comparison (Hwang et al., 2007) for volume fractions greater than 0.1%, Pak and Cho's model is not applicable, while Brinkman's model is more consistent with experimental results.

Xuan and Li (Xuan & Li, 2003) have conducted an experimental investigation on cupper-water nanofluid. Turbulent flow in a tube for Reynolds number between 10000 and 25000 with solid volume fraction ranging from 0.3% to 2% indicated

enhancement of convective heat transfer coefficient with flow velocity as well as solid volume fraction (ϕ). They observed 39% increase in Nusselt number while increasing cupper particle concentration from 0% to 2% at constant Reynolds number. An experimental research on graphite-oil nanofluid by Yang et al. (Yang, Zhang, Grulke, Anderson, & Wu, 2005) for laminar flow in a horizontal tube heat exchanger revealed increase in static thermal conductivity. The enhancement of heat transfer coefficient was less than predicted by conventional correlations. Heris et al. (Heris, Esfahany, & Etemad, 2007) studied laminar flow, forced convection of Al_2O_3-water nanofluid experimentally in a circular tube with constant wall temperature. The thermal conductivity of nanofluid was calculated using the renovated Maxwell model (W. Yu & Choi, 2003) with liquid layer thickness as 10% of Al_2O_3 particle radius. It was observed that heat transfer increased with increase of Peclet number as well as ϕ. The heat transfer coefficient increase was much higher than predicted by heat transfer correlation applicable to the single phase fluid with nanofluid properties. A numerical investigation on γAl_2O_3-water nanofluid has been conducted by Roy et al. (Roy, Nguyen, & Lajoie, 2004) in a radial flow cooling system. They have observed 100% increase in heat transfer by 10 % increase in nanoparticle volume fraction. γAl_2O_3 is cubic aluminum oxide particle. They also found that wall shear stress increases as ϕ increases. Maiga et al. (Maiga, Nguyen, Galanis, & Roy, 2004) have studied laminar flow of γAl_2O_3-water and γAl_2O_3-ethylene glycol nanofluids numerically in a tube with constant wall heat flux. They observed noticeable increase of heat transfer with increase in ϕ. The rate the heat transfer increase was higher for γAl_2O_3-EG. Wall shear stress also increased with ϕ. The increase of wall shear stress was also more for γAl_2O_3-EG than γAl_2O_3-water.

In the present work the forced convection of Cu-water nanofluid in a two dimensional rectangular duct is investigated numerically for both constant wall temperature and constant wall heat flux using single phase model. The nanofluid is considered as an incompressible Newtonian fluid. To determine the thermal conductivity of nanofluid and its effective viscosity model proposed by Patel et al. (Patel et al., 2005) and Brinkman's model (Brinkman, 1952) have been applied respectively.

Chapter 3

MATHEMATICAL MODELING FOR TWO PHASE FLOW

3.1 Introduction

In this chapter the governing continuity, momentum, and energy equations for a two-dimensional parallel plate channel are presented. Corresponding thermal conductivity and viscosity models for copper-water nanofluid is presented. Two Nusselt numbers are defined based on inlet temperature and nanofluid bulk temperature. The boundary conditions at top and bottom walls, channel entrance, and channel outlet are given in this chapter. A brief explanation about the numerical approach, momentum interpolation method, and the discretization scheme is presented in the last part of this chapter.

3.2 Geometry and Problem Statement

Figure 3.1 displays the problem geometry which is a rectangular duct of height H=1cm, and length L=1m with very large depth compared to the height. 'u' and 'v' show axial and vertical velocity components respectively. The cold nanofluid enters the duct at left boundary and leaves it at right. Both cases of uniform and parabolic entrance velocities have been considered. Energy equation has been solved for both constant temperature and constant heat flux boundary conditions at the upper and lower plates (more information about boundary conditions is provided later on this chapter, section 3.4).
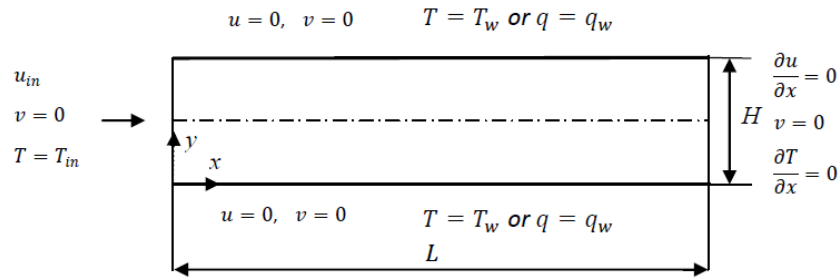
Figure 3.1: Channel Geometry

Copper water is going to be used as nanofluid with spherical particles of uniform shape and size. The nanoparticle diameter is taken to be 100nm. The fluid flow is incompressible, steady state, and laminar and the nanofluid is assumed to be Newtonian. Particle distribution is homogeneous and solid liquid particles are in thermal equilibrium and flow at the same velocity. The hydrodynamic and thermophysical properties of particles and fluid is assumed to be constant and the values are considered at a fixed temperature of $0°C$ which are presented in Table 3.1. Buoyancy force is neglected because of small effect compared to flow, so the problem is a pure forced convection problem.

Table 3.1: Thermophysical properties of water and Cu at $0°C$ ((Jiji, 2006), (Incropera, Lavine, & DeWitt, 2011))

	$\rho (kg/m^3)$	$C_p (J/kg\ K)$	k (W/m K)	$\mu\ (kg/m\ s)$
Pure water	999.8	4218	0.5619	1.791×10^{-3}
Cu	8933	371	406	

3.3 Governing Equations

The governing equations of continuity, momentum, and energy in dimensional form for a two-dimensional problem have been solved. The working fluid is considered to be a mixture of pure water and nanoparticles and treated as a single fluid. Buoyancy

13

effect has been neglected as a result of high flow velocity. The general governing equations are as follow:

Continuity:

$$\frac{\partial \rho_{nf}}{\partial t} + div(\rho_{nf} \vec{V}) = 0 \qquad\qquad 3.1$$

Momentum-X:

$$\frac{\partial (\rho_{nf} u)}{\partial t} + div(\rho_{nf} u\vec{V}) = -\frac{\partial P}{\partial x} + div(\mu_{nf} \, gradu) \qquad\qquad 3.2$$

Momentum-Y:

$$\frac{\partial (\rho_{nf} v)}{\partial t} + div(\rho_{nf} v\vec{V}) = -\frac{\partial P}{\partial y} + div(\mu_{nf} \, gradv) \qquad\qquad 3.3$$

Energy:

$$\frac{\partial (\rho_{nf} C_{p_{nf}} T)}{\partial t} + div(\rho_{nf} C_{p_{nf}} \vec{V}T) = div(k_{eff} \, gradT) \qquad\qquad 3.4$$

Nanofluid density is obtained as follows:

$$\rho_{nf} = (1 - \phi)\rho_f + \phi\rho_p \qquad\qquad 3.5$$

where the subscript nf refers to nanofluid and ϕ is nanoparticle volume fraction. Heat capacity of nanofluid is given by Xuan et al. (Xuan & Roetzel, 2000) as:

$$C_{p_{nf}} = \frac{(1-\phi)\rho_f C_{p_f} + \phi\rho_p C_{p_p}}{\rho_{nf}} \qquad\qquad 3.6$$

Brinkman's model (Brinkman, 1952) is used for effective viscosity of nanofluid.

$$\mu_{nf} = \frac{\mu_f}{(1-\phi)^{2.5}} \qquad\qquad 3.7$$

Effective thermal conductivity of nanofluid is determined using Patel et al.'s model (Patel et al., 2005). For two-phase mixture the model gives

$$\frac{k_{eff}}{k_f} = 1 + \frac{k_p A_p}{k_f A_f} + c k_p Pe \frac{A_p}{k_f A_f} \qquad\qquad 3.8$$

Here c is the only empirical constant of the model. Santra et al. (Santra, Sen, & Chakraborty, 2009) has found it for Cu-water nanofluid from the experimental data obtained by Xuan and Li (Xuan & Li, 2000). The average value of the constant is 3.64×10^4.

Heat transfer area ratio of particle to fluid is calculated as

$$\frac{A_p}{A_f} = \frac{d_f}{d_p} \frac{\phi}{(1-\phi)} \qquad\qquad 3.9$$

Where A_f is the conduction heat transfer area of liquid medium and A_p is the corresponding area of solid particles. Here d_p is the solid particles diameter and d_f is taken as the molecular size of the liquid (2 Å for water (Patel et al., 2005)).

15

Peclet number is given as

$$Pe = \frac{u_p d_p}{\alpha_f} \qquad\qquad 3.10$$

u_p is the Brownian motion velocity of the particles which is given by

$$u_p = \frac{2K_b T}{\pi \mu_f d_p{}^2} \qquad\qquad 3.11$$

where K_b is the Boltzmann constant ($K_b = 1.3807 \times 10^{-23}\,{}^{J}/{}_{K}$).

Thermal diffusivity of nanofluid is

$$\alpha_{nf} = \frac{k_{eff}}{\rho_{nf} C_{p_{nf}}} \qquad\qquad 3.12$$

Local and average Nusselt number at bottom hot wall have been calculated using two different definitions based on the difference between the wall and bulk temperatures. The definitions for both cases of constant wall temperature and constant wall heat flux are given in the following sections.

3.3.1 Nusselt Number for Constant Wall Temperature

3.3.1.1 Nu Based on T_{in}:

Heat flux at the wall boundary is

$$q = h(T_w - T_{in}) = -k_{eff} \left.\frac{\partial T}{\partial y}\right|_{y=0}$$

16

$$\rightarrow h = -k_{eff} \frac{\frac{\partial T}{\partial y}\big|_{y=0}}{T_w - T_{in}} \qquad \text{(a)}$$

Nusselt number for nanofluids is defined in terms of the conductivity of pure fluid as:

$$Nu = \frac{h\, L_{ref}}{k_f} \qquad \text{(b)}$$

Substituting h from (a) to (b) we have

$$Nu_x = -L_{ref} \frac{k_{eff}}{k_f} \frac{\frac{\partial T}{\partial y}\big|_{y=0}}{(T_w - T_{in})} \qquad\qquad 3.13$$

Where, L_{ref} is the reference length and is equal to the width of channel (h) and k_{eff} is a function of x.

The average Nusselt number will be:

$$\overline{Nu} = \frac{1}{L} \int_0^L Nu_x\, dx \qquad\qquad 3.14$$

3.3.1.2 Nu Based on T_b

$$Nu_x = -L_{ref} \frac{k_{eff}}{k_f} \frac{\frac{\partial T}{\partial y}\big|_{y=0}}{(T_w - T_b)} \qquad\qquad 3.15$$

Bulk temperature (T_b) at any cross section of the channel is calculated as:

$$T_b = \frac{\int_{A_c} \rho_{nf} C_{p_{nf}} u\, T\, dA_c}{\int_{A_c} \rho_{nf} C_{p_{nf}} u\, dA_c} \tag{3.16}$$

In this case the average Nusselt number will be a function of x as well:

$$\overline{Nu} = \frac{1}{x} \int_0^x Nu_x\, dx \tag{3.17}$$

3.3.2 Nusselt Number for Constant Wall Heat Flux

3.3.2.1 Nu Based on T_{in}

$$Nu_x = \frac{-q_w L_{ref}}{k_f (T_w - T_{in})} \tag{3.18}$$

$$\overline{Nu} = \frac{1}{L} \int_0^L Nu_x\, dx \tag{3.19}$$

3.3.2.2 Nu Based on T_b

$$Nu_x = \frac{-q_w L_{ref}}{k_f (T_w - T_b)} \tag{3.20}$$

$$\overline{Nu} = \frac{1}{L} \int_0^L Nu_x\, dx \tag{3.21}$$

Shear stress at the bottom wall is:

$$\tau_x = \mu_{nf} \left.\frac{\partial u}{\partial y}\right|_{y=0} \tag{3.22}$$

While the average wall shear stress is:

$$\bar{\tau} = \frac{1}{L} \int_0^L \tau_x \, dx \qquad\qquad 3.23$$

Reynolds number is defined by:

$$Re = \frac{\rho_f \, U_{ref} \, H}{\mu_f} \qquad\qquad 3.24$$

Where H is channel width and $U_{ref} = U_m$ is the mean inlet velocity.

and Re_{D_e} as following:

$$Re_{D_e} = \frac{\rho_f \, U_{ref} \, D_e}{\mu_f} \qquad\qquad 3.25$$

where D_e (equivalent diameter) is given by:

$$D_e = \frac{4 \, A_f}{P} = 2H \qquad\qquad 3.26$$

Using equations 3.26, 3.27, and 3.28 we have:

$$Re_{D_e} = 2 \, Re \qquad\qquad 3.27$$

3.4 Boundary Conditions

Governing equations used in this work are two-dimensional partial differential equations in Cartesian coordinates. Boundary conditions, used to solve momentum equations are uniform or parabolic velocity profiles at the entrance, fully developed velocity profile at the outlet, and no slip boundary condition at top and bottom walls.

For the energy equation, flow enters the channel at a low uniform temperature and leaves it while it is thermally developed. Wall boundary conditions are constant temperature and constant heat flux cases.

3.4.1 Entrance Boundary Conditions

Uniform entrance velocity:

At $x=0$, $0 \leq y \leq H$: $u = u_m$, $v=0$, $T = T_c$

Where u_m is the mean velocity at the inlet.

with $u_m = 1\ m/s$ and $T_c = 0°C$

Parabolic entrance velocity:

At $x=0$, $0 \leq y \leq H$: $u(y) = \frac{-6u_m}{H^2} y^2 + \frac{6u_m}{H} y$, $v=0$, $T = T_c$

with $u_m = 1\ m/s$ and $T_c = 0°C$

3.4.2 Outlet Boundary Conditions

For all variables zero gradient condition have been considered at the outlet:

At $x=L$, $0 \leq y \leq H$: $\frac{\partial u}{\partial x} = 0$, $\frac{\partial v}{\partial x} = 0$, $\frac{\partial T}{\partial x} = 0$

and to ensure overall mass conservation, correcting the axial velocity component at the outlet is necessary:

$$u_{N,j} = u_{N-1,j}\ \frac{\dot{m}_{in}}{\dot{m}_{out}}$$

where N refers to a point at the outlet boundary, and

$\dot{m}_{in} = \int_A \rho_{nf}\ u_{in}\, dA$ and $\dot{m}_{out} = \int_A \rho_{nf}\ u_{N,j}\, dA$

3.4.3 Wall Boundary Conditions

Constant wall temperature:

At $y=0$, $0 \leq x \leq L$: $u=0$, $v=0$, $T = T_h$

At $y=H$, $0 \leq x \leq L$: $u=0$, $v=0$, $T = T_h$

with $T_h = 1°C$

Constant wall heat flux:

At $y=0$, $0 \leq x \leq L$: $u=0$, $v=0$, $q = q_w$

At $y=H$, $0 \leq x \leq L$: $u=0$, $v=0$, $q = q_w$

with $q_w = 10$ $W/_{m^2}$

3.5 Numerical Method

A Fortran code has been developed to find the velocity and temperature profile of a flow in a rectangular channel.

Mass, momentum, and energy conservation equations have been discretized by a control volume approach. The general form of differential equations for a steady state fluid flow is as following:

$$\underbrace{\frac{\partial(\rho_{nf}\,u\varphi)}{\partial x} + \frac{\partial(\rho_{nf}\,v\varphi)}{\partial y}}_{\text{Convection term}} = \underbrace{\frac{\partial}{\partial x}\left(\Gamma\frac{\partial\varphi}{\partial x}\right) + \frac{\partial}{\partial y}\left(\Gamma\frac{\partial\varphi}{\partial y}\right)}_{\text{Diffusion term}} + \underbrace{S_\varphi}_{\text{Source term}} \qquad 3.28$$

21

With $\varphi = 1$ and $\Gamma = 0$ in continuity equation, $\varphi = u$ or v and $\Gamma = \mu_{nf}$ in momentum conservation equation, and $\varphi = T$ and $\Gamma = \frac{k_{eff}}{C_{p_{nf}}}$ in energy equation.

The diffusion term is discretized using central difference scheme, while CUBISTA scheme (Convergent and Universally Bounded Interpolation Scheme for Treatment of Advection) (Alves, Oliveira, & Pinho, 2003) is used to discretize the convection term. This is a TVD (total-variation diminishing) high resolution scheme (HRS) with third order accuracy. The face value for uniform meshes in this scheme is given by:

$$\varphi_f = \begin{cases} \frac{7}{4}\hat{\varphi}_P & 0 < \hat{\varphi}_P < \frac{3}{8} \\[2mm] \frac{3}{4}\hat{\varphi}_P + \frac{3}{8} & \frac{3}{8} \le \hat{\varphi}_P \le \frac{3}{4} \\[2mm] \frac{1}{4}\hat{\varphi}_P + \frac{3}{4} & \frac{3}{4} < \hat{\varphi}_P < 1 \\[2mm] \hat{\varphi}_P & \text{elsewhere} \end{cases} \qquad 3.29$$

Transforming the relations for the case of non-uniform meshes gives:

$$\varphi_f = \begin{cases} [1 + \frac{\check{X}_f - \check{X}_P}{3(1-\check{X}_P)}]\frac{\check{X}_f}{\check{X}_P}\hat{\varphi}_P & 0 < \hat{\varphi}_P < \frac{3}{4}\check{X}_P \\[3mm] \frac{\check{X}_f(1-\check{X}_f)}{\check{X}_P(1-\check{X}_P)}\hat{\varphi}_P + \frac{\check{X}_f(\check{X}_f-\check{X}_P)}{1-\check{X}_P} & \frac{3}{4}\check{X}_P \le \hat{\varphi}_P \le \frac{1+2(\check{X}_f-\check{X}_P)}{2\check{X}_f-\check{X}_P}\check{X}_P \\[3mm] 1 - \frac{1-\check{X}_f}{2(1-\check{X}_P)}(1-\hat{\varphi}_P) & \frac{1+2(\check{X}_f-\check{X}_P)}{2\check{X}_f-\check{X}_P}\check{X}_P < \hat{\varphi}_P < 1 \\[3mm] \hat{\varphi}_P & \text{elsewhere} \end{cases} \qquad 3.30$$

where

$$\hat{X}_P = \frac{X_P - X_U}{X_D - X_U} \quad , \quad \hat{X}_f = \frac{X_f - X_U}{X_D - X_U}$$

and

$$\hat{\varphi}_P = \frac{\varphi_P - \varphi_U}{\varphi_D - \varphi_U} \quad , \quad \hat{\varphi}_f = \frac{\varphi_f - \varphi_U}{\varphi_D - \varphi_U}$$

Here *X* stands for *x* or *y* coordinates and the subscripts *U* and *D* refer to upstream and downstream cells to cell *P* which is, itself, upstream of the cell face *f* under consideration.

Since non-staggered (collocated) grid system has been employed the problem of checker board pressure field has been avoided by using momentum interpolation method (B. Yu et al., 2002), and to find the pressure profile the SIMPLE algorithm has been employed.
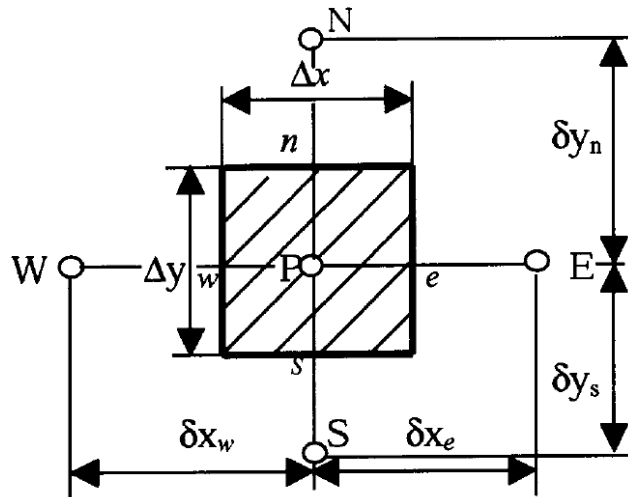

Figure 3.2: Nonstaggered grid arrangement

Discretizing any of continuity, momentum, or energy equations with general variable *φ* gives:

$$A_P \varphi_P = A_E \varphi_E + A_W \varphi_W + A_N \varphi_N + A_S \varphi_S + b_P \qquad \text{3.31}$$

where

$$A_E = \frac{\Gamma_e \Delta y}{\delta x_e} + \max[-(\rho u)_e \Delta y, 0] \qquad A_W = \frac{\Gamma_w \Delta y}{\delta x_w} + \max[(\rho u)_w \Delta y, 0]$$

$$A_N = \frac{\Gamma_n \Delta x}{\delta y_n} + \max[-(\rho v)_n \Delta x, 0] \qquad A_S = \frac{\Gamma_s \Delta x}{\delta y_s} + \max[(\rho v)_s \Delta x, 0]$$

and

$$A_P = A_E + A_W + A_N + A_S - S_P + \Delta F \qquad \text{3.32}$$

here

$$\Delta F = (\rho u)_e \Delta y - (\rho u)_w \Delta y + (\rho v)_n \Delta x - (\rho v)_s \Delta x \qquad \text{3.33}$$

and

$$b_P = S_C + b_1 \qquad \text{3.34}$$

where

$$\begin{aligned}
b_1 = &- \max[(\rho u)_e \Delta y, 0] \, (\varphi_e - \varphi_P) + \max[-(\rho u)_e \Delta y, 0] \, (\varphi_e - \varphi_E) \\
&- \max[-(\rho u)_w \Delta y, 0] \, (\varphi_w - \varphi_P) + \max[(\rho u)_w \Delta y, 0] \, (\varphi_w - \varphi_W) \\
&- \max[(\rho v)_n \Delta x, 0] \, (\varphi_n - \varphi_P) + \max[-(\rho v)_n \Delta x, 0] \, (\varphi_n - \varphi_N) \\
&- \max[-(\rho v)_s \Delta x, 0] \, (\varphi_s - \varphi_P) + \max[(\rho v)_s \Delta x, 0] \, (\varphi_s - \varphi_S) \qquad \text{3.35}
\end{aligned}$$

Here $\varphi_e, \varphi_w, \varphi_n$, and φ_s are being calculated using abovementioned CUBISTA method and u_e, u_w, v_n, and v_s are being found using momentum interpolation method (B. Yu et al., 2002). The following equation shows the calculation of u_e (similar relations are being used for other faces).

$$
u_e = \frac{1}{(A_P)_e} \left\{
\begin{array}{l}
[f_e^+(A_P)_E u_E + (1 - f_e^+)(A_P)_P u_P] \\[6pt]
+\alpha_u[(f_e^+(S_c)_E + (1 - f_e^+)(S_c)_P)\delta x_e \Delta y \\[6pt]
-f_e^+(S_c)_E \Delta x_E \Delta y - (1 - f_e^+)(S_c)_P \Delta x_P \Delta y] \\[6pt]
+\alpha_u[-\Delta y(P_E - P_P) + f_e^+ \Delta y(P_e - P_w)_E \\[6pt]
+(1 - f_e^+)\Delta y(P_e - P_w)_P] \\[6pt]
+(1 - \alpha_u)[u_e^0(A_P)_e - f_e^+ u_E^0(A_P)_E - (1 - f_e^+)u_P^0(A_P)_P]
\end{array}
\right.
\qquad 3.36
$$

where $(A_P)_e$ is being interpolated as:

$$
(A_P)_e = f_e^+(\textstyle\sum_i A_i)_E + (1 - f_e^+)(\textstyle\sum_i A_i)_P - [f_e^+(S_P)_E + (1 - f_e^+)(S_P)_P]\delta x_e \Delta y \quad 3.37
$$

and

$$
f_e^+ = \frac{\Delta x}{2\delta x_e}
$$

Here superscript 0 refers to previous iteration and subscripts e and w refer to east and west faces respectively and subscript E refers to east cell. α_u stands for axial velocity under relaxation factor.

Chapter 4

RESULTS AND DISCUSSION

4.1 Introduction

The heat transfer problem associated with the flow between two parallel plates has been studied numerically for a two phase flow with symmetric top and bottom thermal boundary conditions. The geometry of the problem is presented in Fig. 3.1. The channel is 1 m in length while the height is 1 cm. The nanofluid is composed of water as base fluid with copper particles of 100 nm diameter suspended in it. The flow and temperature fields are studied for a range of *Re* and ϕ. Thermal conductivity of nanofluid has been calculated using Patel et. al.'s correlation for each control volume as it depends on temperature. The constant 'c' in the correlation has been calculated from experimental results for copper-water nanofluid (Xuan & Li, 2000). The average value of constant is used in our work, which is 3.60×10^4. Thermophysical properties of water and copper at the base temperature, i.e. at $0°C$ are summarized in Table 3.1. Results are presented and compared for both cases of uniform and parabolic entrance velocity while the walls are kept at constant temperature and constant heat flux. *Re* changes from 10 to 1500 while ϕ has been varied from 0 to 5 %.

4.2 Grid Independence Study

A grid independence study has been conducted for the solution domain and the variation in wall average Nusselt number and shear stress have been recorded for different grids. The calculations were made for pure fluid in channel with uniform

26

entrance velocity and walls at constant heat flux. It is found that 201 grids along X-direction by 41 grids along Y-direction give satisfactory results. Further increase in the number of grids does not affect the results noticeably. The results of the grid independence study have been summarized in Table 4.1.

The wall average Nusselt number and shear stress are given by equations 3.19 and 3.23, respectively.

Table 4.1: Results of grid independence test, at *Re*=500, pure fluid

No. of grids in X-direction	No. of grids in Y-direction	Average Nu number at the bottom wall	Average wall shear stress
201	21	5.845399	3.2129262×10^{-2}
301	21	5.843040	3.2136444×10^{-2}
401	21	5.842008	3.2136366×10^{-2}
501	21	5.841102	3.2149129×10^{-2}
601	21	5.842097	3.2100447×10^{-2}
201	31	5.923468	3.2372497×10^{-2}
301	31	5.920895	3.2393817×10^{-2}
401	31	5.919976	3.2391556×10^{-2}
501	31	5.920148	3.2413919×10^{-2}
601	31	5.919202	3.2422930×10^{-2}
201	41	5.954765	3.2463636×10^{-2}
301	41	5.952280	3.2502819×10^{-2}
401	41	5.951772	3.2533895×10^{-2}
201	81	5.986251	3.2574236×10^{-2}
401	81	5.985945	3.2616271×10^{-2}

4.3 Validation of Code

The local wall Nusselt numbers (based on T_b) defined by equations 3.15 and 3.20 , respectively for channel with constant wall temperature and constant wall heat flux have been compared with the analytical solution given by Das et al. (R. Das & Mohanty, 1983) for pure fluid and uniform entrance velocity. With Prandtl number (*Pr*) and non-dimensional axial distance (ζ) given by:

$$Pr = \frac{\mu_f C_{p_f}}{k_f} \qquad\qquad 4.1$$

$$\zeta = \frac{2\,x}{H\,Re} \qquad\qquad 5.1$$

The results for two cases of constant wall temperature and constant wall heat flux have been summarized in Table 4.2 and Table 4.3 respectively. The percentage deviations from theoretical values are presented for each case.

4.3.1 Constant Wall Temperature

Table 4.2: Local wall Nusselt number for clear fluid, constant wall temperature, comparison with theoretical results

ζ	Nu_X , Pr=0.1			Nu_X , Pr=1.0			Nu_X , Pr=10		
	(R. Das & Mohanty,	Present Study	Deviation (%)	(R. Das & Mohanty, 1983)	Present Study	Deviation (%)	(R. Das & Mohanty, 1983)	Present Study	Deviation (%)
0.002	5.566	6.042	8.55	11.603	12.765	10.015	26.197	26.633	1.664
0.0053	4.280	4.538	6.03	7.913	8.226	3.956	16.930	16.993	0.372
0.029	4.015	3.905	-2.740	4.420	4.577	3.552	8.495	8.707	2.495
0.048	3.985	3.832	-3.839	3.977	4.095	2.967	7.250	7.322	0.993
0.057	3.974	3.811	-4.102	3.973	3.983	0.252	6.854	6.924	1.02
0.470				3.934	3.766	-4.270	3.976	4.120	3.622

4.3.2 Constant Wall Heat Flux

Table 4.3: Local wall Nusselt number for clear fluid, constant wall heat flux, comparison with theoretical results

ζ	Nu_X , Pr=0.1			Nu_X , Pr=1.0			Nu_X , Pr=10		
	(R. Das & Mohanty,	Present Study	Deviation (%)	(R. Das & Mohanty,	Present Study	Deviation (%)	(R. Das & Mohanty,	Present Study	Deviation (%)
0.002	6.893	8.172	18.555	15.330	16.916	10.345	31.740	35.639	12.284
0.0085	4.379	5.064	15.643	8.378	8.983	7.221	17.471	18.641	6.697
0.020	4.242	4.443	4.738	5.912	6.487	9.726	12.058	13.051	8.235
0.057	4.156	4.181	0.602	4.352	4.752	9.189	8.248	8.767	6.296
0.071	4.143	4.153	0.241	4.146	4.539	9.490	7.647	8.125	6.249
0.660				4.117	4.113	-0.097	4.158	4.525	8.826

It has been observed that the percentage deviation from analytical solution for channel with constant wall temperature remains below 10.015% while 18.56 % deviation has been observed for channel with constant heat flux for small values of *Pr* and ζ.

4.4 Effect of Various Parameters on Local and Average Nusselt Numbers (Based on T_{in} and T_b)

4.4.1 Effect of Solid Volume Fraction and Reynolds Number on Local Wall Nusselt Number (Based on T_{in})

4.4.1.1 Constant Wall Temperature, and Uniform Entrance Velocity

The local Nusselt number based on T_{in} is shown in Fig. 4.1 and Fig. 4.2 at constant wall temperature and uniform inlet velocity for $Re=100$ and $Re=1500$ respectively.
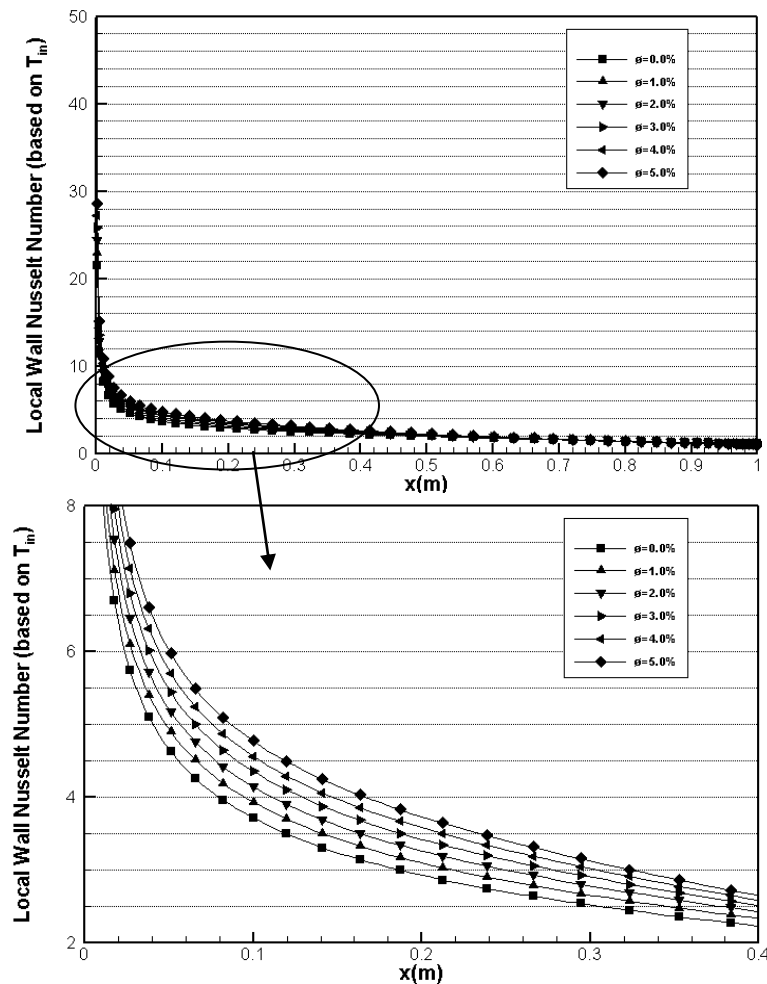
Figure 4.1: Distribution of local Nusselt number at hot wall for different solid volume fractions, $Re=100$
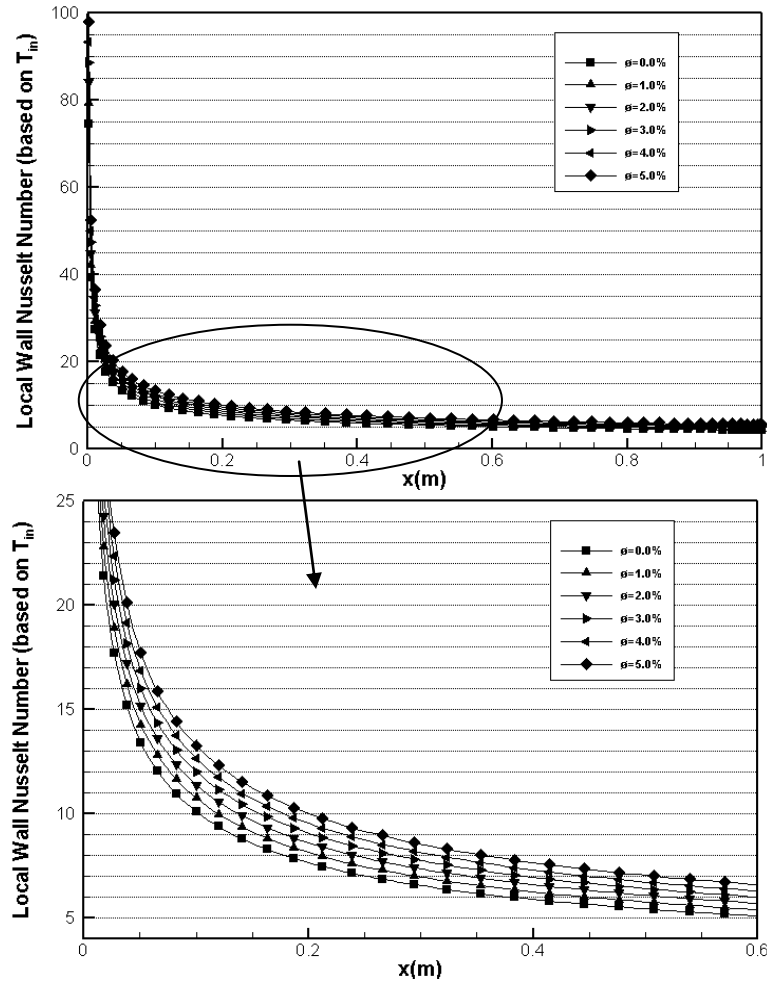
Figure 4.2: Distribution of local Nusselt number at hot wall for different solid
volume fractions, *Re*=1500

The local wall Nusselt number based on T_{in} decreases with axial distance (x) in the parallel plates channel where a magnified view near the entrance is also included in the figure. As the nanofluid temperature in the vicinity of walls approaches to the the wall temperature along the axial direction, $\frac{\partial T}{\partial y}$ decreases, which results in the reduction of the local Nusselt number. As indicated in the picture the local Nusselt number increases as nanoparticle volume fraction increases. The increase in Nusselt number with nanoparticle volume fraction is a result of enhancement of thermal conductivity of nanofluid with ϕ which causes higher convection heat transfer.

32

Figure 4.3 depicts the local Nusselt number based on T_{in} at constant wall temperature and uniform inlet velocity for $\phi=2.5\%$.
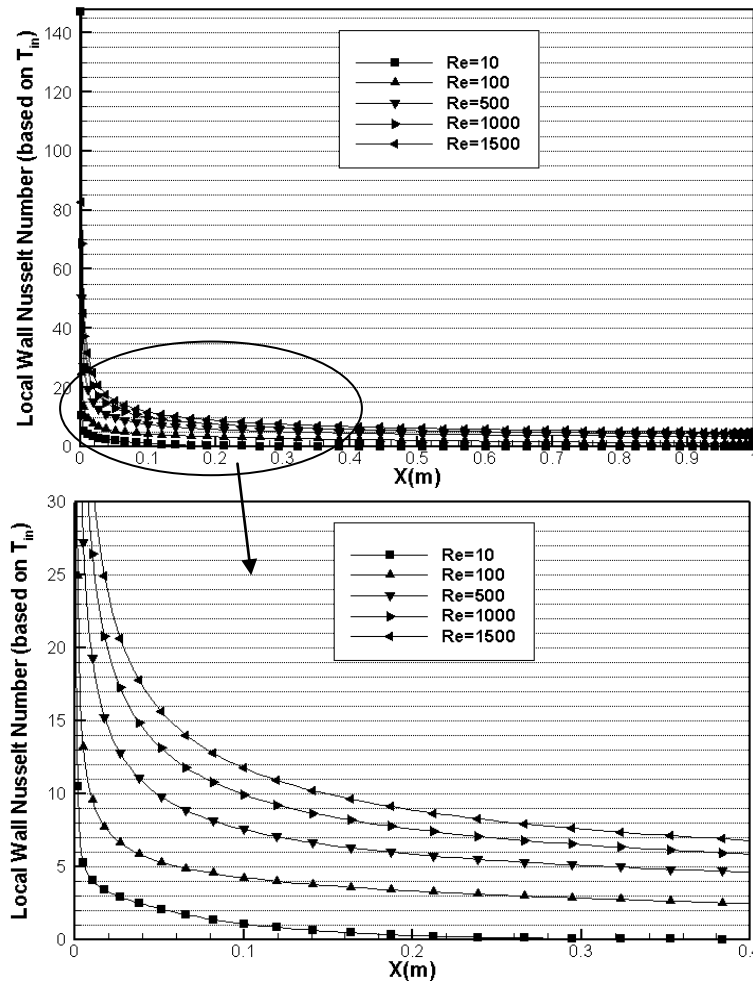
Figure 4.3: Distribution of local Nusselt number at hot wall for different Reynolds numbers, $\phi=2.5\%$.

Higher local Nusselt number is observed for higher values of Reynolds number at a constant solid volume fraction in Fig. 4.3 which is a result of higher heat transport from the surface at higher fluid velocities.

33

4.4.1.2 Constant Wall Temperature, Comparison Between, Uniform and Parabolic Entrance Velocities

The local Nusselt number based on T_{in} is shown in Fig. 4.4 and Fig. 4.5 at constant wall temperature for uniform and parabolic inlet velocities for $Re=100$ and $Re=1000$ respectively.
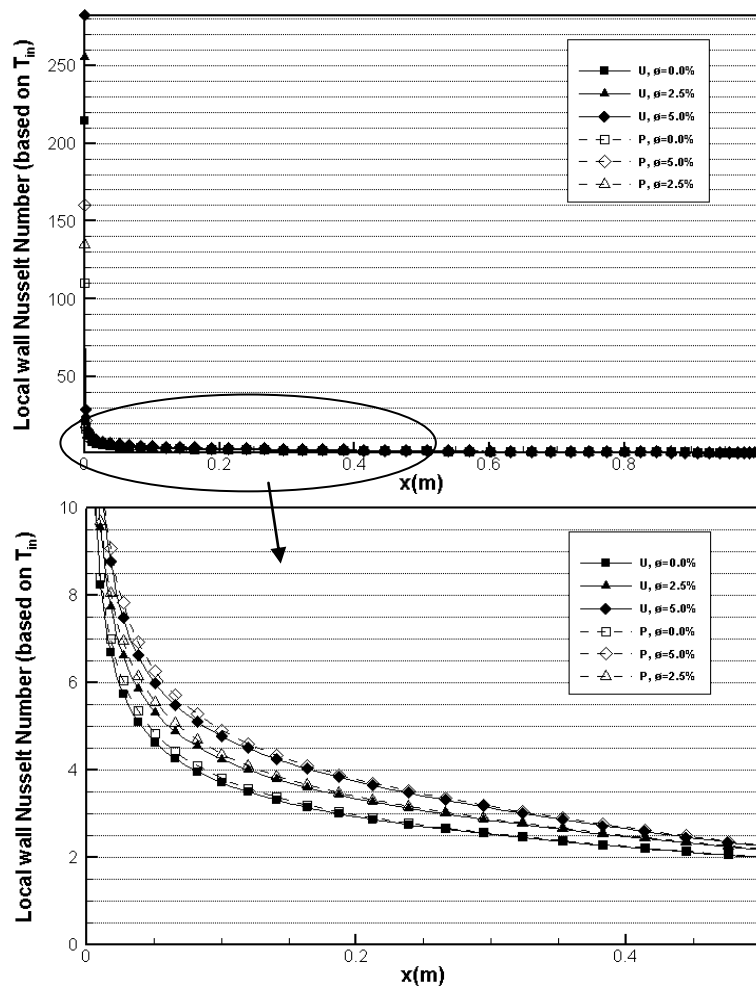
Figure 4.4: Comparison of local Nusselt number along hot wall between uniform (U) and parabolic (P) entrance velocities, different solid volume fractions, $Re=100$
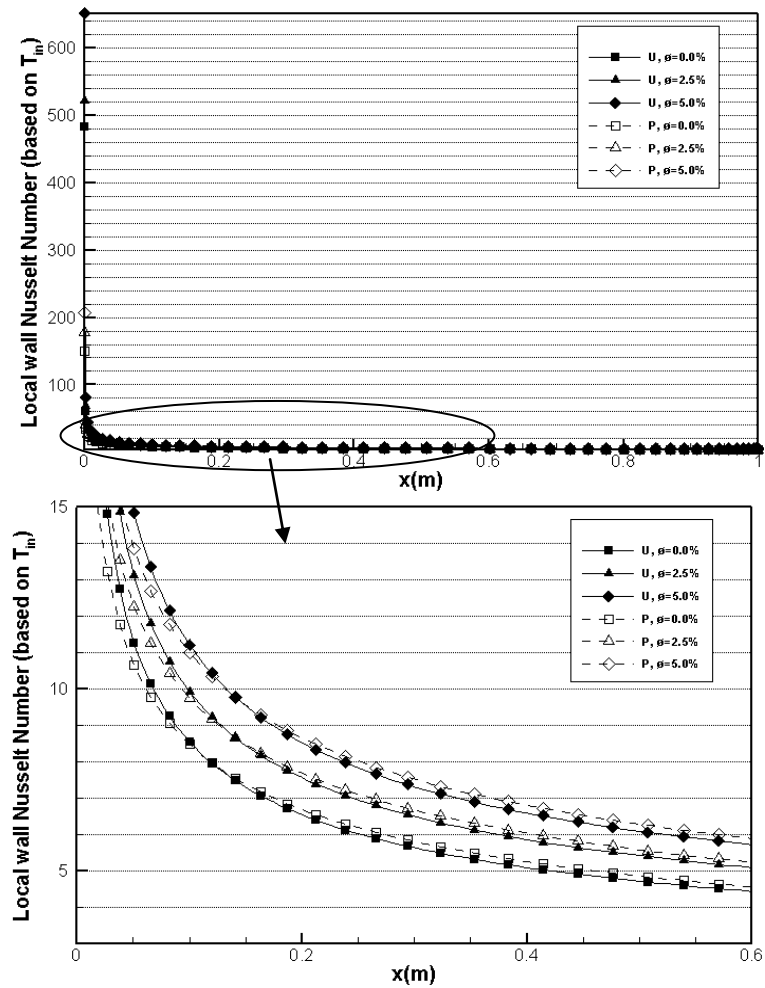
Figure 4.5: Comparison of local Nusselt number along hot wall between uniform (U) and parabolic (P) entrance velocities, different solid volume fractions, *Re*=1000

The local Nusselt numbers for channel with parabolic entrance velocity show the same trend of changes as channel with uniform entrance velocity. As shown in Fig. 4.4 and Fig. 4.5, the local Nusselt number decreases with x and increases with solid volume fraction at constant Reynolds number. As depicted in the figure, the channel with uniform entrance velocity, shows higher values of local Nusselt number close to the flow entrance region but, at all solid volume fractions, this difference decreases with *x* until the Nusselt number values for channel with parabolic entrance velocity exceeds the other.

Figure 4.6 depicts the local Nusselt number based on T_{in} at constant wall temperature, for uniform and parabolic inlet velocities for $\phi=2.5\%$.
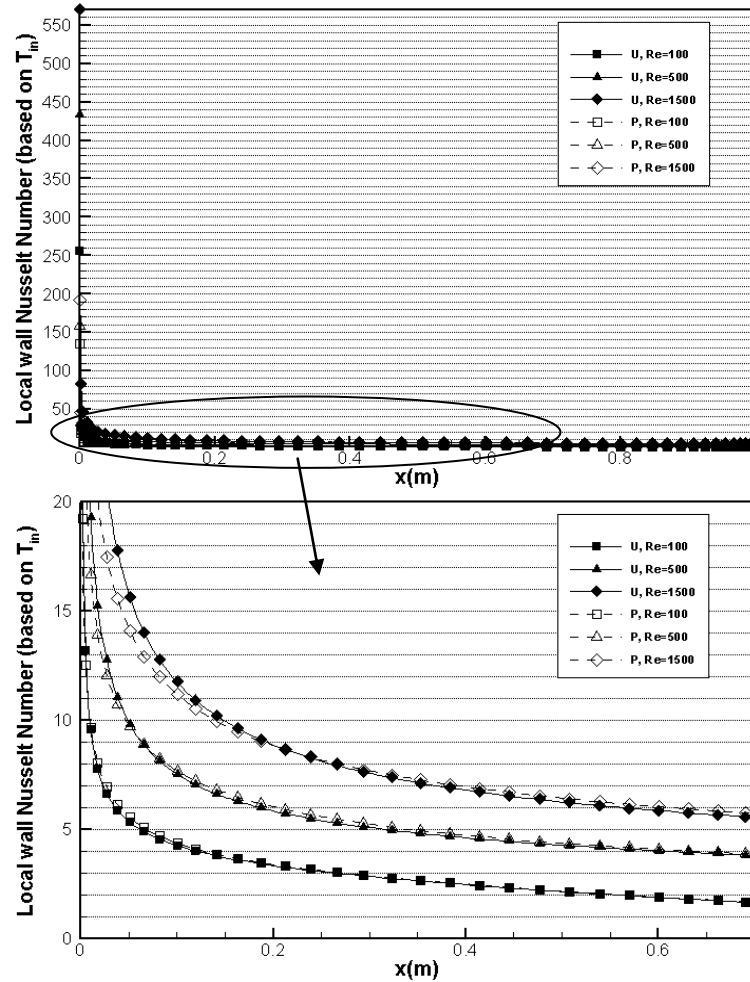
Figure 4.6: Comparison of local Nusselt number along hot wall between uniform (U) and parabolic (P) entrance velocities, different Reynolds numbers, $\phi=2.5\%$

Similar to channel with uniform entrance velocity an increase in local Nusselt number with Reynolds number has been observed for channel with parabolic entrance velocity (Fig. 4.6). As shown, the channel with uniform entrance velocity, shows higher values of local Nusselt number at smaller values of x but, for all Reynolds numbers, this difference decreases with x until the Nusselt number values for channel with parabolic entrance velocity become larger than the Nusselt values for channel with uniform entrance velocity.

36

4.4.1.3 Constant Wall Heat Flux, and Uniform Entrance Velocity

The local Nusselt number based on T_{in} is shown in Fig. 4.7 and Fig. 4.8 at constant

wall heat flux and uniform inlet velocity for *Re*=100 and *Re*=1500 respectively.
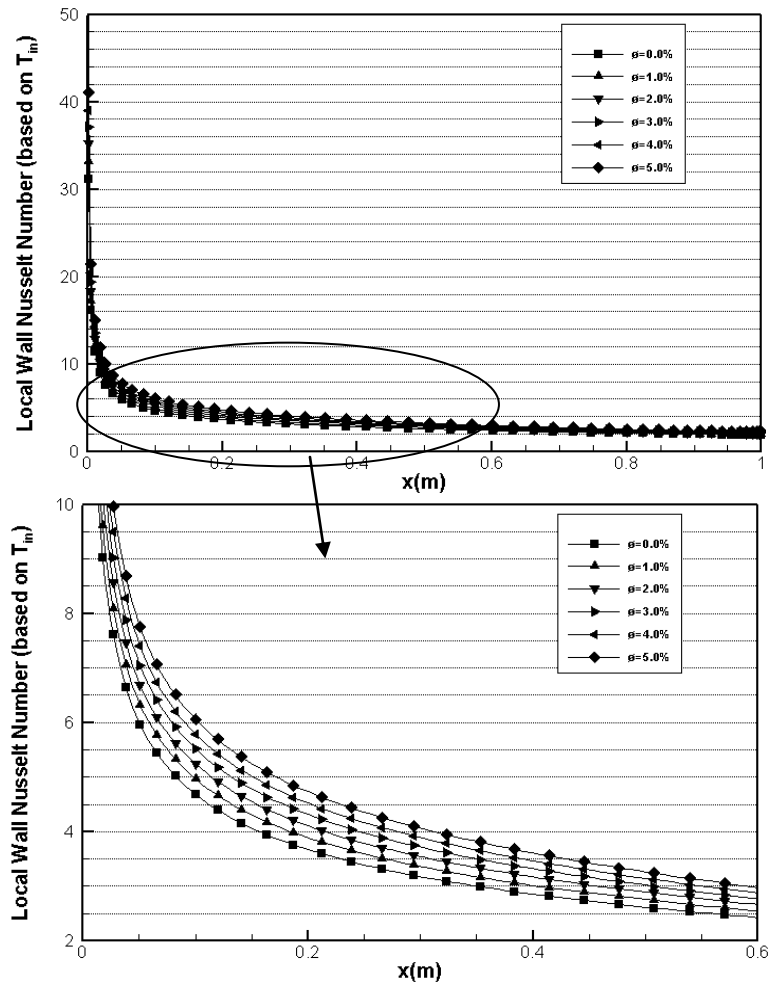
Figure 4.7: Distribution of local Nusselt number at hot wall for different solid
volume fractions, *Re*=100
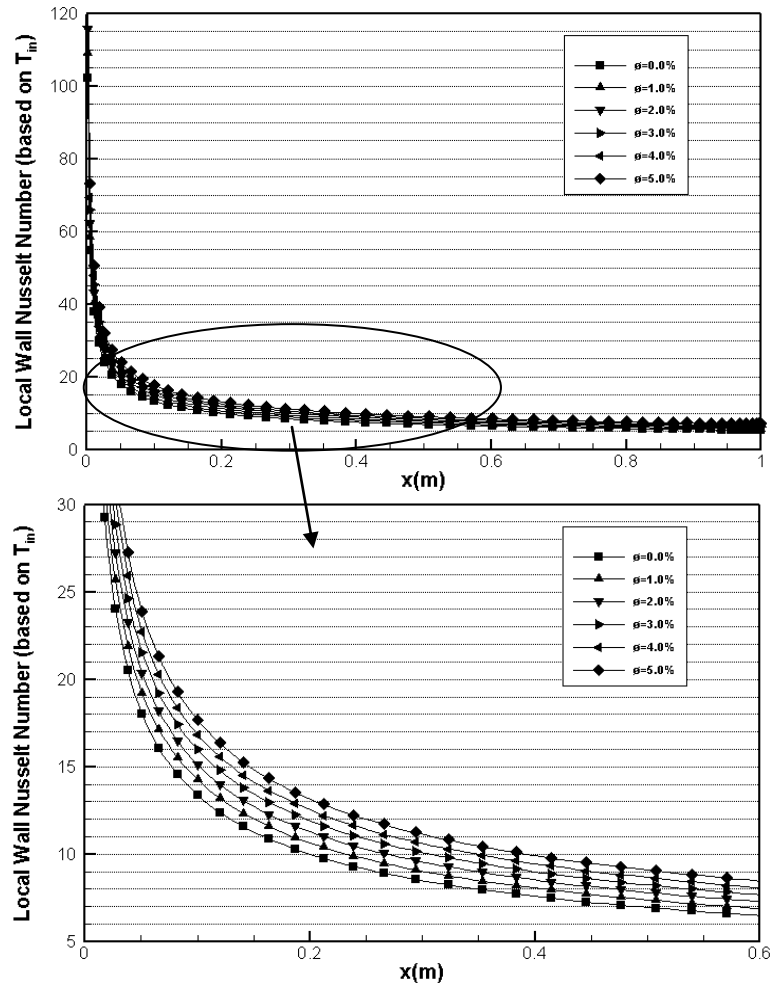
Figure 4.8: Distribution of local Nusselt number at hot wall for different solid
volume fractions, *Re*=1500

As indicated in Fig. 4.7 the local wall Nusselt number based on T_{in} also decreases

with x for the case of walls with constant heat flux. Increasing wall temperature with

x means higher difference between wall and inlet temperature, which causes the local

Nusselt number to fall (Eq. 3.18). At higher values of solid particle volume fraction

higher conductivity of nanofluid increases the rate of heat transfer between the walls

and nanofluid which keeps the wall temperature lower and results in higher values of

local Nusselt number.

Figure 4.9 depicts the local Nusselt number based on T_{in} at constant wall heat flux

and uniform inlet velocity for ϕ=2.5%.

38
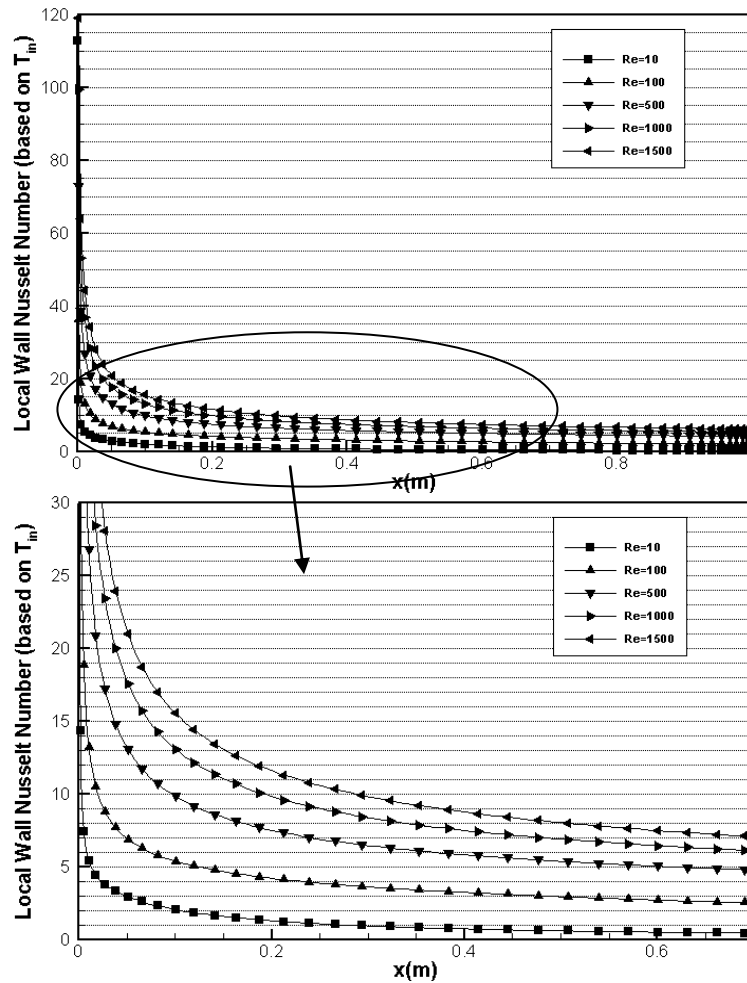
Figure 4.9: Distribution of local Nusselt number at hot wall for different Reynolds numbers, ϕ=2.5%.

As Reynolds number increases higher rate of heat transfer causes the wall temperature to remain lower which enhances the local wall Nusselt number.

4.4.1.4 Constant Wall Heat Flux, Comparison Between, Uniform and Parabolic Entrance Velocities

The local Nusselt number based on T_{in} is shown in Fig. 4.10 and Fig. 4.11 at constant wall heat flux for uniform and parabolic inlet velocities for Re=100 and Re=1000 respectively.
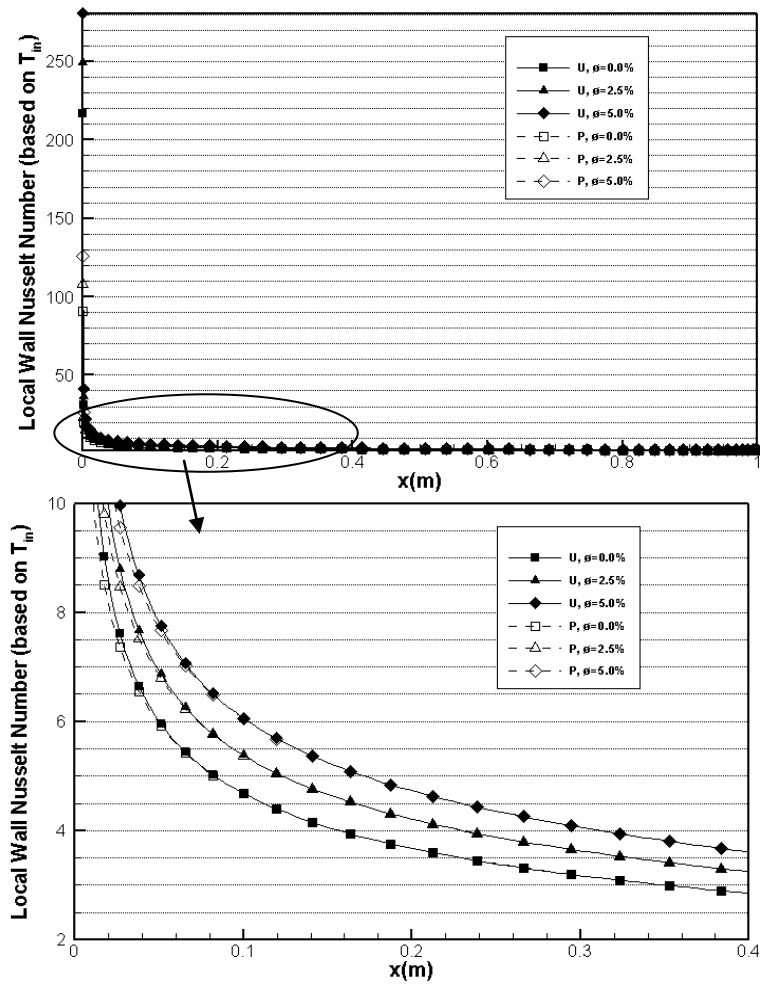
Figure 4.10: Comparison of local Nusselt number along hot wall between uniform (U) and parabolic (P) entrance velocities, different solid volume fractions, *Re*=100
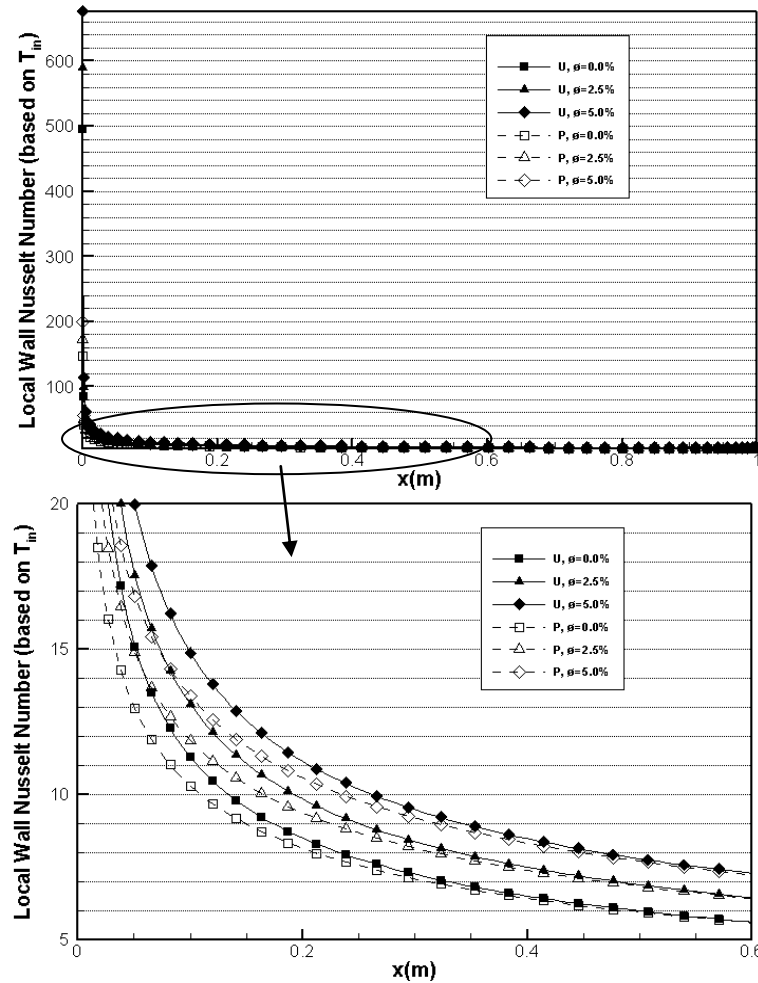
Figure 4.11: Comparison of local Nusselt number along hot wall between uniform (U) and parabolic (P) entrance velocities, different solid volume fractions, *Re*=1000

The same course of changes as channel with uniform entrance velocity is observed for channels at constant heat flux in Fig 4.10 and Fig. 4.11. The local Nusselt decreases with x and increases with ϕ.

As depicted in the figure, the channel with uniform entrance velocity, shows higher values of local Nusselt number close to the flow entrance region but, for all values of solid volume fraction, this difference decreases with *x* until the Nusselt number values for channel with parabolic entrance velocity exceeds the Nusselt values for channel with uniform entrance velocity.

Figure 4.12 depicts the local Nusselt number based on T_{in} at constant wall heat flux, for uniform and parabolic inlet velocities for ϕ=2.5%.
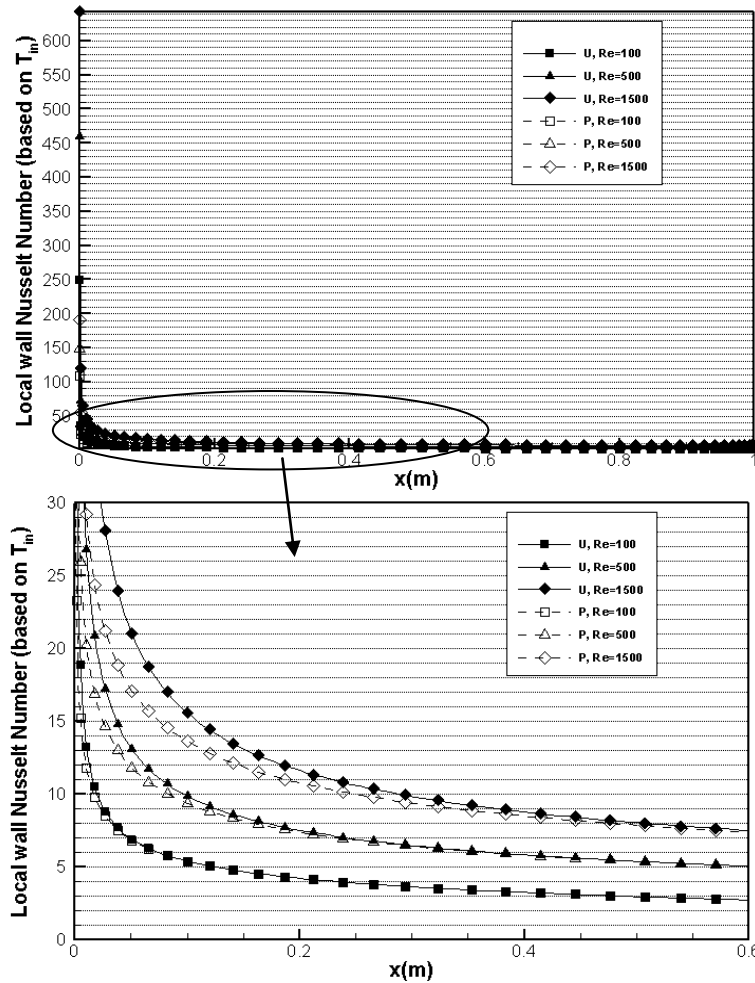
Figure 4.12: Comparison of local Nusselt number along hot wall between uniform (U) and parabolic (P) entrance velocities, different Reynolds numbers, ϕ=2.5%.

In both cases of uniform and parabolic entrance velocities, the local Nusselt number increases with Reynolds number, at a constant value of solid volume fraction.

As shown in Fig. 4.12, the channel with uniform entrance velocity, shows higher values of local Nusselt number at smaller values of x but, for all Reynolds numbers, this difference decreases with x until the Nusselt number values for channel with parabolic entrance velocity become larger than the Nusselt values for channel with uniform entrance velocity.

4.4.2 Average Wall Nusselt Number (Based On T_{in})

4.4.2.1 Constant Wall Temperature

The variation of average Nusselt number with solid volume fraction (ϕ) for different *Re* is presented in Fig. 4.13 for the cases of uniform and parabolic entrance velocities. Here average Nusselt number is calculated based on T_{in} (Eq. 3.14), between *x=0* and *x=L* where *L= 1m*. For all cases the flow is hydrodynamically fully developed at the exit.
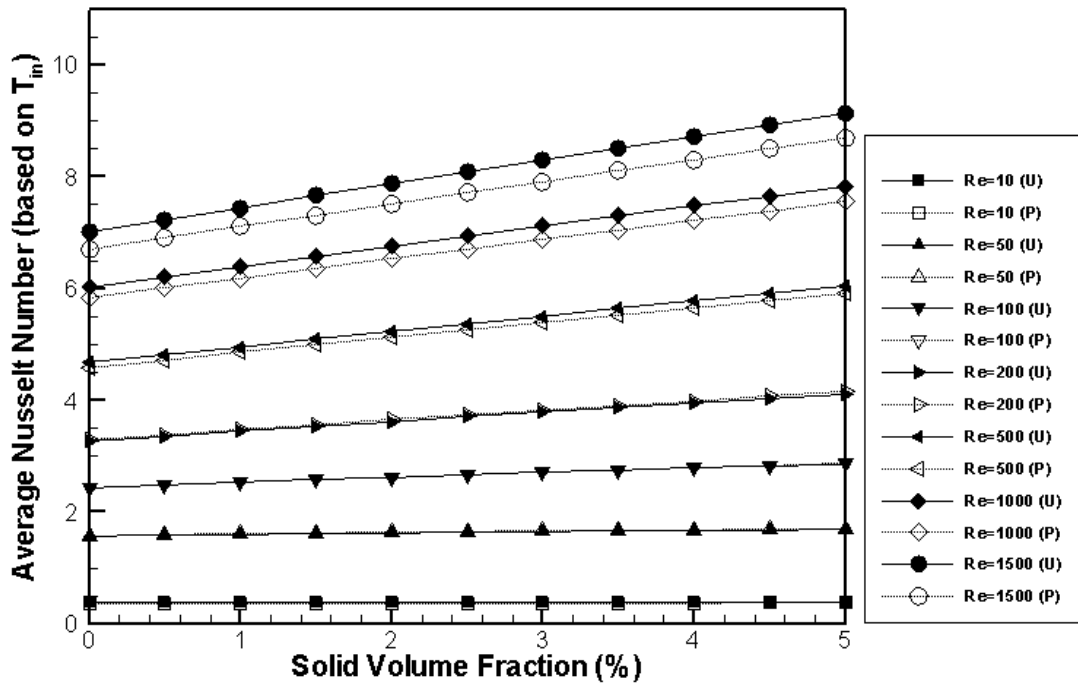
Figure 4.13: Average Nusselt number at hot wall for different *Re* and ϕ for uniform (U) and parabolic (P) entrance velocities, constant wall temperature

As it is shown in Fig. 4.13, $\overline{Nu}$ increases with increment of *Re* as well as ϕ. This is due to rise in effective thermal conductivity of nanofluid with increase in ϕ and increase in convection with the increase in *Re*. At high *Re*, the average wall Nusselt number of channel for the case of uniform inlet velocity is greater than that of parabolic inlet velocity, while at smaller *Re* the difference is small and the graphs nearly overlap. At *Re=1500* and ϕ=5% $\overline{Nu}$ increases by 5% when the entrance

velocity changes from parabolic to uniform. On the other hand this change is 4.4% if a pure fluid is used. This increase in $\overline{Nu}$ for a channel with uniform inlet flow can be interpreted as a result of hydrodynamic entrance region with high local Nu due to developing velocity boundary layer, which is desirable in practical heat transfer applications.

Figure 4.14 illustrates the augmentation of Nusselt ratio of nanofluid to pure fluid $(\overline{Nu_{nf}}/\overline{Nu_f})$ as a function of solid volume fraction (ϕ) for different Reynolds numbers. The results for both cases of uniform and parabolic entrance velocities have been depicted in the figure. In both cases the enhancement of nanofluid Nusselt number is much larger for higher values of Re. That is because, for lower Re due to small flow momentum, the temperature rapidly reaches the wall temperature regardless of the volume fraction of nanoparticles. However at higher Re a continuous increase of Nusselt ratio is evident as ϕ increases. This is due to increase of nanofluid conductivity as a result of increase in solid volume fraction. The Nusselt ratio increase for uniform inlet velocity is smaller than the increase for parabolic inlet velocity at Re=10 while, it is vice versa for Re=1500.

Table 4.4 presents the average Nusselt numbers for various solid volume fractions and Reynolds numbers for channel with uniform entrance velocity. This table shows that for Re=1500, an increase of 5% in the solid volume fraction of nanoparticles results in 30.3% increase in the heat transfer rate. In table 4.5 The average Nusselt numbers for various ϕ and Re for channel with parabolic entrance velocity are presented. In this case 5% increase in solid volume fraction at Re=1500 results in 29.6% increase in $\overline{Nu}$.
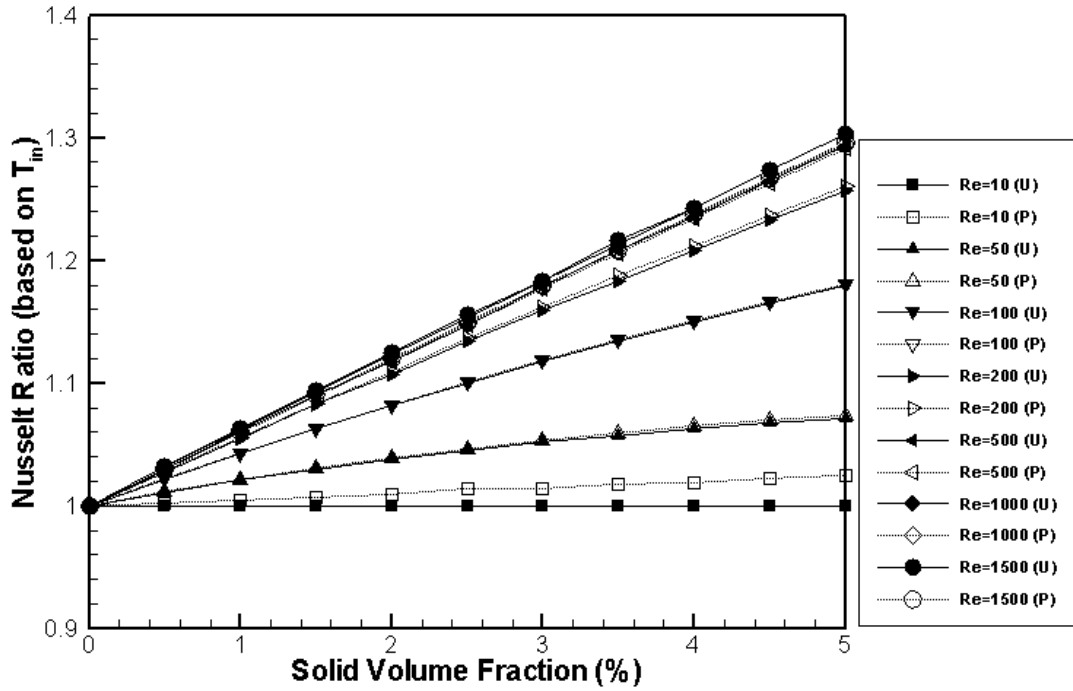
Figure 4.14: uniform (U) and parabolic (P) entrance velocities, $L=1m$, T_w=constant

Table 4.4: Effect of solid volume fraction on the average Nu number ($\overline{Nu}$), uniform entrance velocity

	$\phi = 0\%$	$\phi = 1\%$	$\phi = 2\%$	$\phi = 3\%$	$\phi = 4\%$	$\phi = 5\%$
Re=10	0.380	0.380	0.380	0.380	0.381	0.381
Re=100	2.426	2.530	2.624	2.710	2.789	2.860
Re=500	4.671	4.952	5.225	5.504	5.773	6.048
Re=1500	7.002	7.441	7.879	8.281	8.704	9.123

Table 4.5: Effect of solid volume fraction on the average Nu number ($\overline{Nu}$), parabolic entrance velocity

	$\phi = 0\%$	$\phi = 1\%$	$\phi = 2\%$	$\phi = 3\%$	$\phi = 4\%$	$\phi = 5\%$
Re=10	0.369	0.371	0.373	0.375	0.376	0.379
Re=100	2.426	2.530	2.625	2.712	2.792	2.864
Re=500	4.581	4.854	5.124	5.391	5.654	5.916
Re=1500	6.705	7.110	7.510	7.906	8.299	8.690

45

4.4.2.2 Constant Wall Heat Flux

The variation of average Nusselt number with solid volume fraction (ϕ) for different *Re* is presented in Fig. 4.15 for the cases of uniform and parabolic entrance velocities. The same result has been presented for channel with constant temperature walls. Here average Nusselt number is calculated based on T_{in} (Eq. 3.19), between $x=0$ and $x=L$ where $L=$ 1*m*. For all cases the flow is hydrodynamically fully developed at the exit.
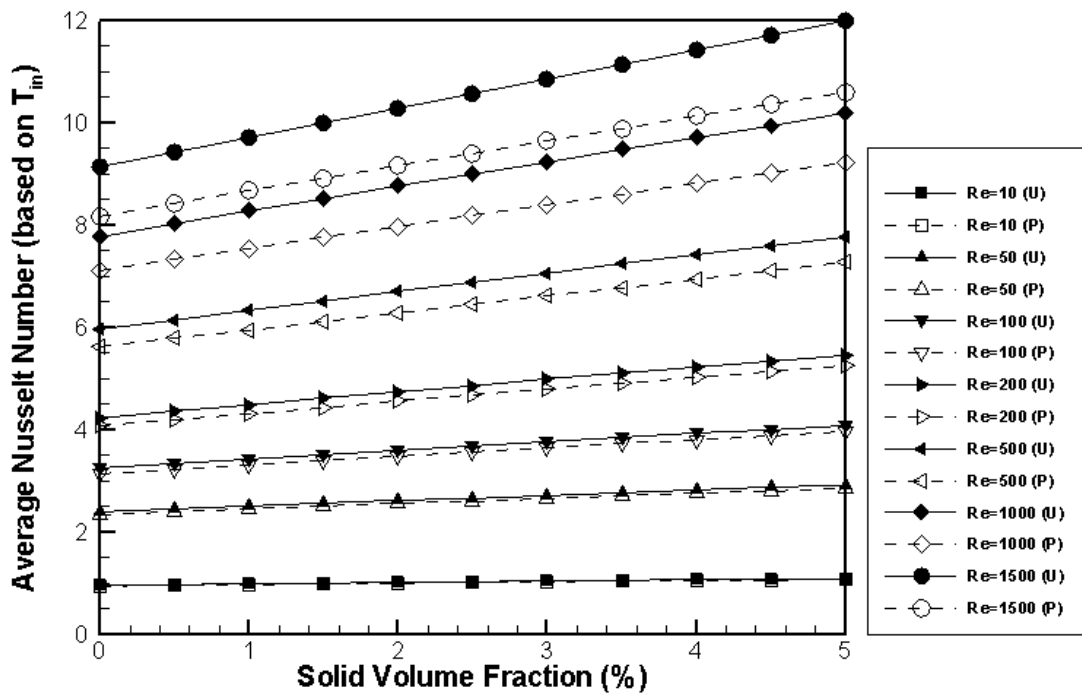

Figure 4.15: Average Nusselt number at hot wall for different *Re* and ϕ for uniform (U) and parabolic (P) entrance velocities, constant wall heat flux

Like the case of constant wall temperature $\overline{Nu}$ increases with *Re* as well as ϕ. At constant *Re* the average Nusselt number is generally greater for channel with uniform entrance velocity as depicted in Fig. 4.15. This difference becomes more noticeable as *Re* increases so that the biggest difference happens at *Re=1500*. At *Re=1500* the

$\overline{Nu}$ increases by 11.7% for pure fluid and 13% for nanofluid with ϕ=5% when entrance velocity changes from parabolic to uniform.

The augmentation of Nusselt ratio $(\overline{Nu_{nf}}/\overline{Nu_f})$ with solid volume fraction (ϕ) is presented in Fig. 4.16 for different Reynolds numbers and for constant wall heat flux. As shown in the figure, the results at smaller values of Re overlap, while at higher Re more increase of Nu ratio is observed for channel with uniform entrance velocity as solid volume fraction increases.

In Table 4.6 and Table 4.7 values are given for channels with uniform and parabolic entrance velocities. Using the values at Re=1500 we come across to a 31.3% and a 30.0% increase of $\overline{Nu}$ respectively for uniform and parabolic inlet velocities as a result of 5% increase in nanoparticle volume fraction.
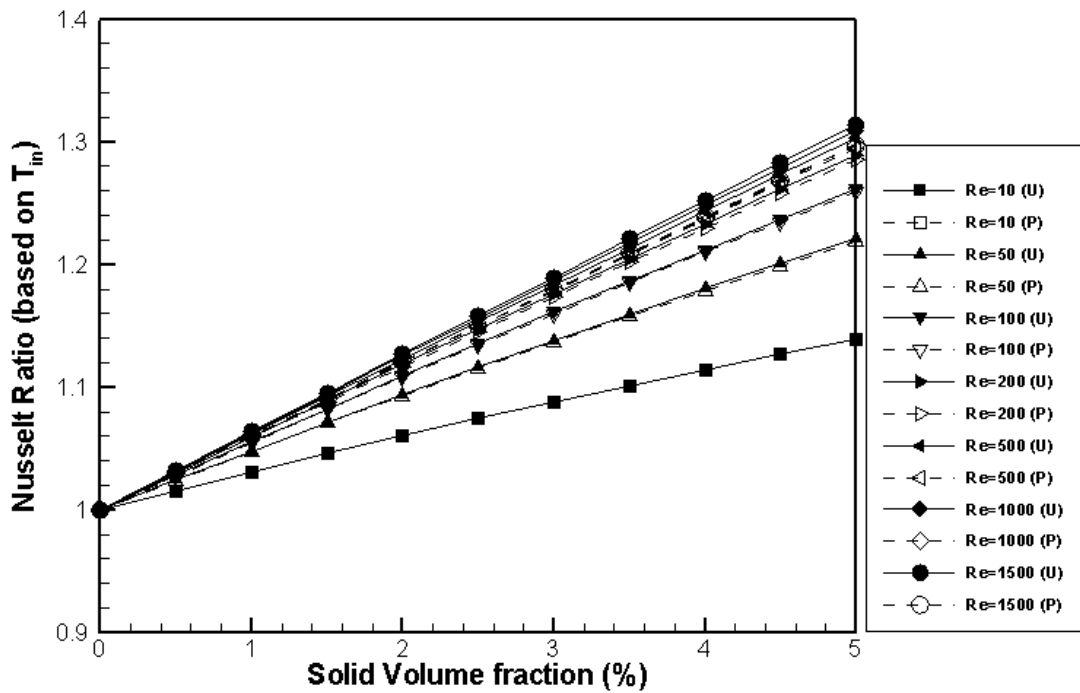
Figure 4.16: uniform (U) and parabolic (P) entrance velocities, L=1m, q_w=constant

Table 4.6: Effect of solid volume fraction on the average Nusselt number ($\overline{Nu}$), uniform entrance velocity

	$\phi = 0\%$	$\phi = 1\%$	$\phi = 2\%$	$\phi = 3\%$	$\phi = 4\%$	$\phi = 5\%$
Re=10	0.960	0.990	1.018	1.045	1.070	1.094
Re=100	3.238	3.417	3.591	3.760	3.924	4.084
Re=500	5.964	6.332	6.696	7.056	7.414	7.769
Re=1500	9.122	9.703	10.279	10.850	11.417	11.981

Table 4.7: Effect of solid volume fraction on the average Nusselt number ($\overline{Nu}$), parabolic entrance velocity

	$\phi = 0\%$	$\phi = 1\%$	$\phi = 2\%$	$\phi = 3\%$	$\phi = 4\%$	$\phi = 5\%$
Re=10	0.946	0.975	1.003	1.029	1.053	1.077
Re=100	3.147	3.320	3.487	3.650	3.808	3.962
Re=500	5.609	5.947	6.280	6.610	6.938	7.263
Re=1500	8.169	8.664	9.154	9.639	10.120	10.599

4.4.2.3 Comparison between Two Cases of Constant Wall Temperature and Constant Wall Heat Flux

Figure 4.17 shows the average Nusselt numbers for the cases of constant wall temperature and constant wall heat flux while channel inlet velocity profile is uniform.
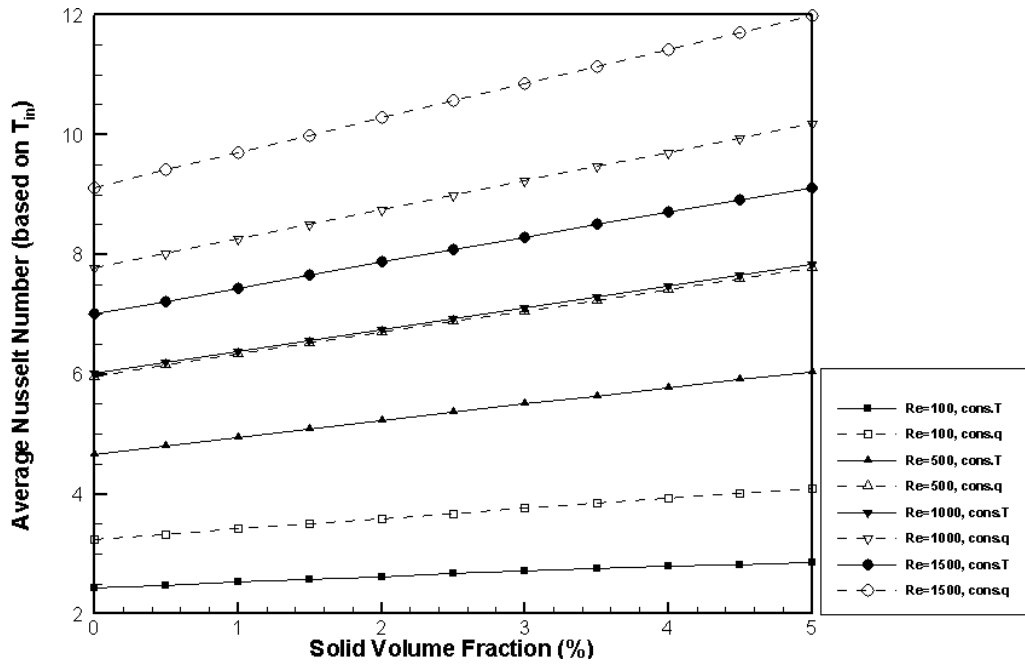
Figure 4.17: Average Nusselt number at hot wall, different *Re* and ϕ, for constant wall temperature (cons. T) and constant wall heat flux (cons. q), channel with uniform entrance velocity

At all *Re* and ϕ values the $\overline{Nu}$ is higher when walls are at constant heat flux. At ϕ=0% and *Re*=100 the $\overline{Nu}$ increases by 33.5% when the wall changes from constant temperature to constant heat flux while at ϕ=0% and *Re*=1500 this increment will be 30.3%. Likewise at ϕ=5% and *Re*=100 the $\overline{Nu}$ increases by 42.8% and at *Re*=1500 by 31.4% when the wall changes from constant temperature to constant heat flux.
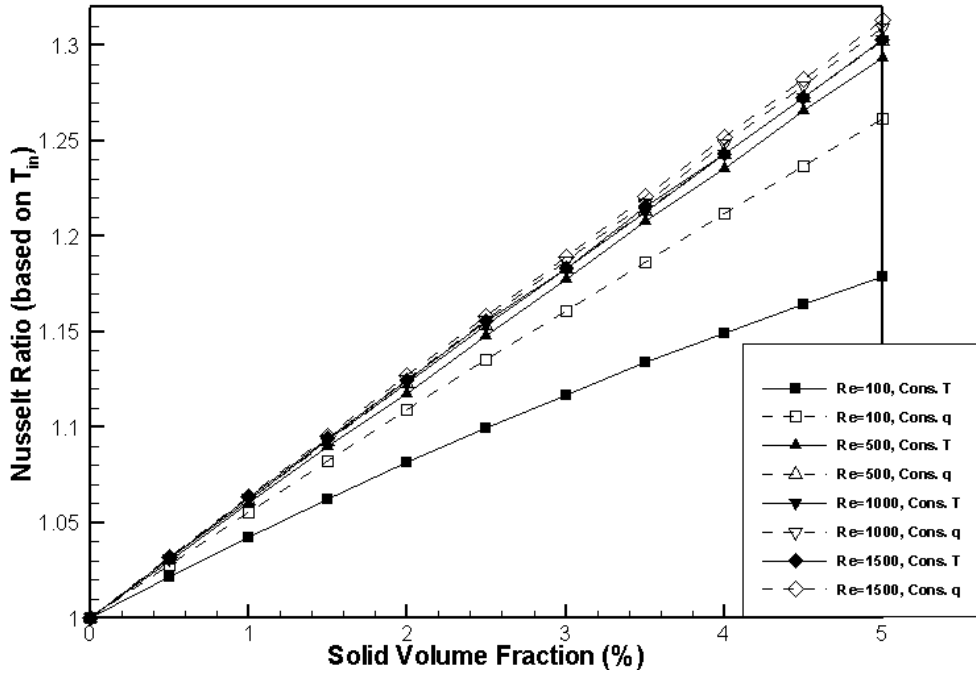
Figure 4.18: walls at constant temperature and constant heat flux, uniform entrance velocity, *L=1m*

The increase of Nusselt ratio $(\overline{Nu_{nf}}/\overline{Nu_f})$ with solid volume fraction (ϕ) is presented in Fig. 4.18 for different Reynolds numbers and for uniform entrance velocity when walls are considered at both constant temperature and constant heat flux.

More increase of Nusselt ratio with nanoparticle volume fraction is observed for channel with walls at constant heat flux, compared to the channel with walls at constant temperature. This difference is higher at lower values of Reynolds number. At *Re*=100 we come across to 17.9% and 26.1% increase in $\overline{Nu}$, respectively for walls at constant temperature and constant heat flux, as a result of 5% increase in nanoparticle volume fraction. While at Re=1500 these increments are 30.3% and 31.3%.

In Fig. 4.19 the change of average Nusselt number (based on T_{in}) is shown with particle volume fraction. The results for two cases of walls at constant temperature and constant heat flux are compared while the entrance velocity profile is parabolic.
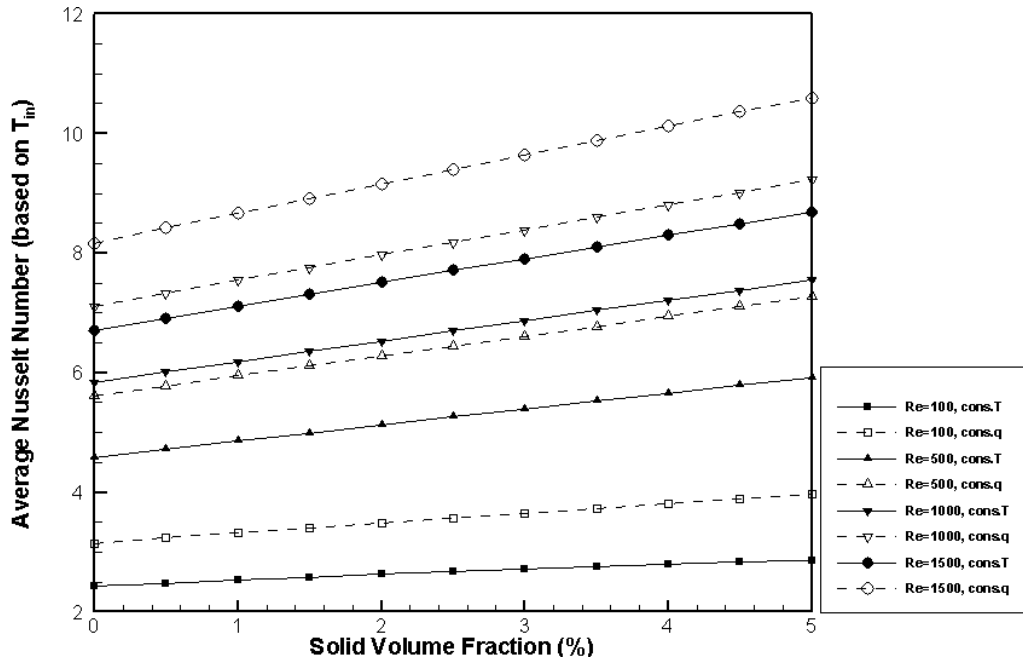

Figure 4.19: Average Nusselt number at hot wall, different Re and ϕ, for constant wall temperature (cons. T) and constant wall heat flux (cons. q), channel with parabolic entrance velocity

Similar to the case of channel with uniform entrance velocity at all Re and ϕ values the $\overline{Nu}$ is higher when walls are at constant heat flux. At ϕ=0% and Re=100 the $\overline{Nu}$ increases by 29.7% when the wall changes from constant temperature to constant heat flux while at ϕ=0% and Re=1500 this increment will be 21.8%. Likewise at ϕ=5% and Re=100 the $\overline{Nu}$ increases by 38.3% and at Re=1500 by 22% when the wall changes from constant temperature to constant heat flux.

Figure 4.20 shows the increase of Nusselt ratio $(\overline{Nu_{nf}}/\overline{Nu_f})$ with solid volume fraction (ϕ) for different Reynolds numbers when inlet velocity profile is parabolic, and for walls at constant temperature and constant heat flux.

51
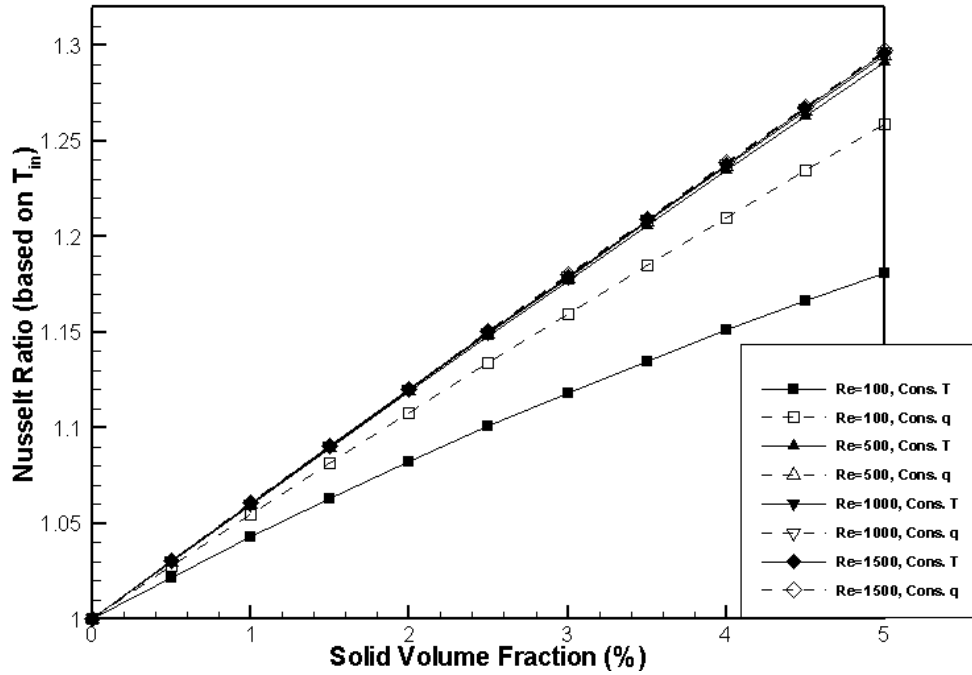
Figure 4.20: walls at constant temperature and constant heat flux, parabolic entrance velocity, $L=1m$

When walls are at constant heat flux, more increase of Nusselt ratio with nanoparticle volume fraction is observed compared to the case of walls at constant temperature. This difference is higher at lower Re. At $Re=100$, 18.1% and 25.9% increase in $\overline{Nu}$ is observed, respectively for walls at constant temperature and constant heat flux, as a result of 5% increase in nanoparticle volume fraction. While at Re=1500 these increments are 29.6% and 29.7%.

4.4.3 Local and Average Wall Nusselt Numbers (Based on T_b)

Here local and average Nusselt numbers based on local bulk temperature T_b are given respectively by equations 3.15 and 3.17 for walls at constant temperature and by equations 3.20 and 3.21 for walls at constant heat flux. Results are presented for a pure fluid.

4.4.3.1 Constant Wall Temperature

Local and average Nusselt numbers (based on T_b) with respect to ξ for pure fluid flow in channel with walls at constant temperature are shown in Fig. 4.21 and Fig.

4.22, for uniform and parabolic inlet velocities respectively, for different values of Reynolds numbers.
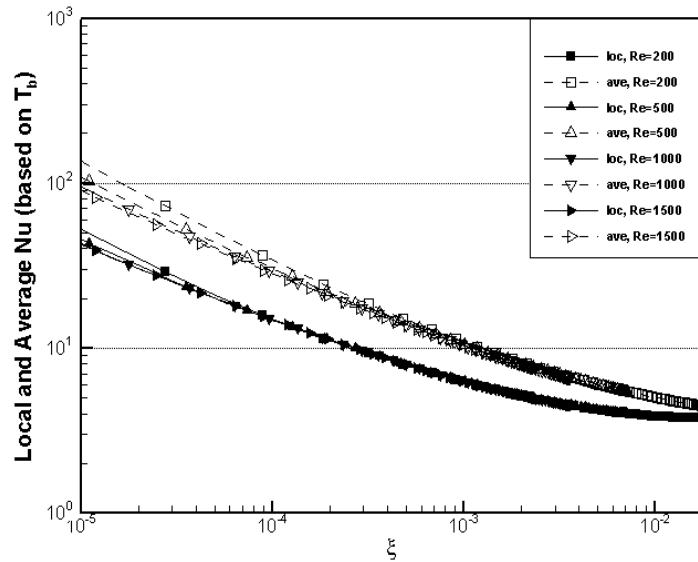
Figure 4.21: Local and average Nusselt number vs $\xi = \frac{x/D_e}{Re_{D_e}Pr}$ for different Reynolds numbers, uniform entrance velocity for a pure fluid (ϕ=0.0%)
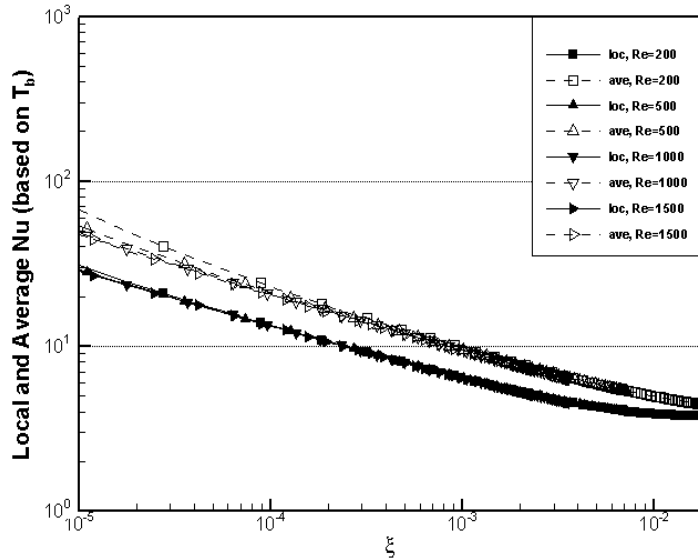
Figure 4.22: Local and average Nusselt number vs $\boldsymbol{\xi = \frac{x/D_e}{Re_{D_e}Pr}}$ for different Reynolds numbers, parabolic entrance velocity for a pure fluid (ϕ=0.0%)

The local and average Nusselt numbers defined by Eq. 3.15 and 3.17 have to overlap for different values of Reynolds number, but as indicated in the pictures, there are some scatter of data close to the entrance region of the channel for smaller values of

Re. In both cases of uniform and parabolic entrance velocities the local and average

Nusselt numbers converge to 3.7 ($Nu|_{\xi \to \infty} = \overline{Nu}|_{\xi \to \infty} = 3.7$).

In the following pictures (Fig. 4.23 and Fig. 4.24) The local and average Nusselt

numbers (based on T_b) have been compared for two cases of uniform and parabolic

entrance velocities while walls are at constant temperature for a pure fluid.
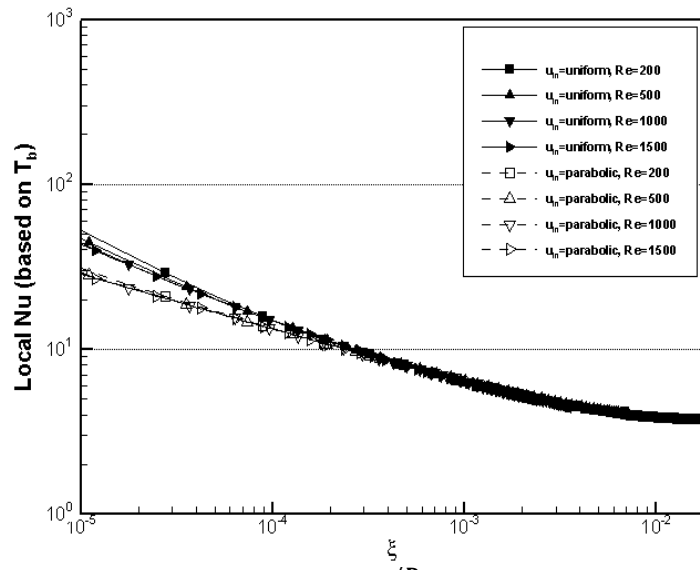
Figure 4.23: Local Nusselt number vs $\boldsymbol{\xi} = \dfrac{x/D_e}{Re_{D_e} Pr}$ for uniform and parabolic entrance velocities and different Reynolds numbers for a pure fluid (ϕ=0.0%)
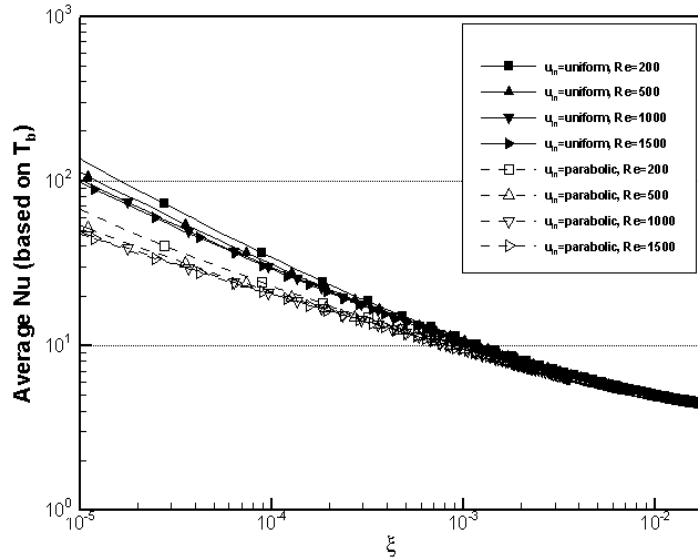
Figure 4.24: Average Nusselt number vs $\xi = \dfrac{x/D_e}{Re_{D_e}Pr}$ for uniform and parabolic entrance velocities and different Reynolds numbers for a pure fluid ($\phi=0.0\%$)

Average Nusselt numbers (based on T_b) with respect to ξ for pure fluid flow in channel with walls at constant temperature are shown in Fig. 4.24, for uniform and parabolic inlet velocities, for different values of Reynolds numbers.

As seen in Fig. 4.23 and Fig. 4.24 the local and average Nusselt numbers are higher for channel with uniform entrance velocity, compared to the channel with parabolic entrance velocity at smaller values of ξ while for higher values of ξ, they converge to the same value of 3.7.

Local and average Nusselt number ratios (based on T_b) of the nanofluid (with $\phi=5\%$) to pure fluid, are shown in Fig. 4.25 and Fig. 4.26 for channel with uniform and parabolic inlet velocities respectively, where walls are at constant temperature.
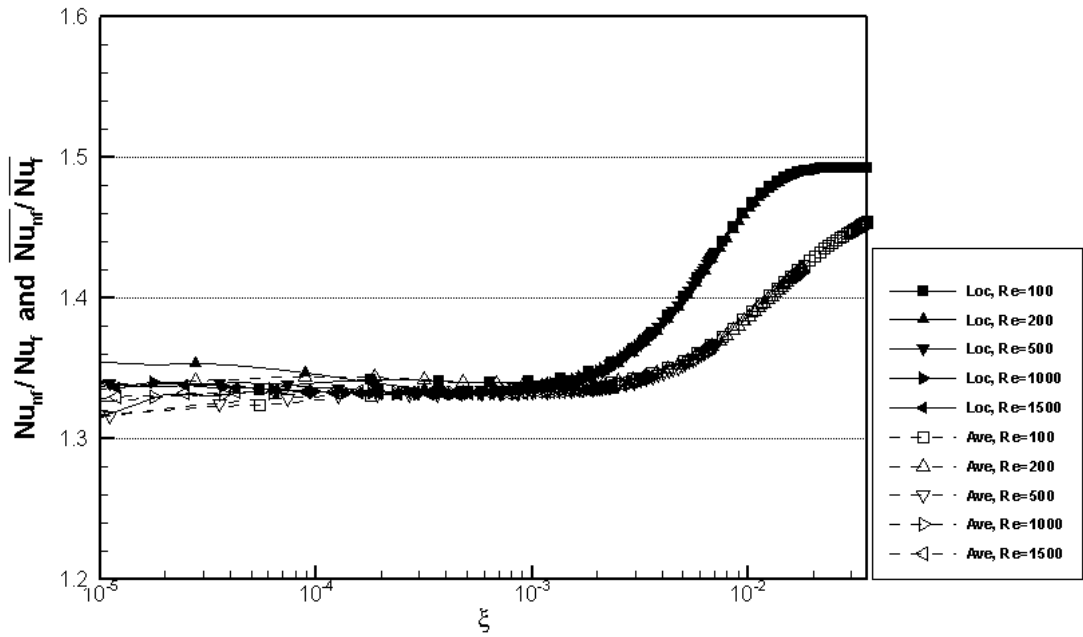
Figure 4.25: Local (Loc) and average (Ave) Nusselt number ratios, vs $\xi = \dfrac{x/D_e}{Re_{D_e}Pr}$ for uniform entrance velocity and constant wall temperature for ϕ=5.0%
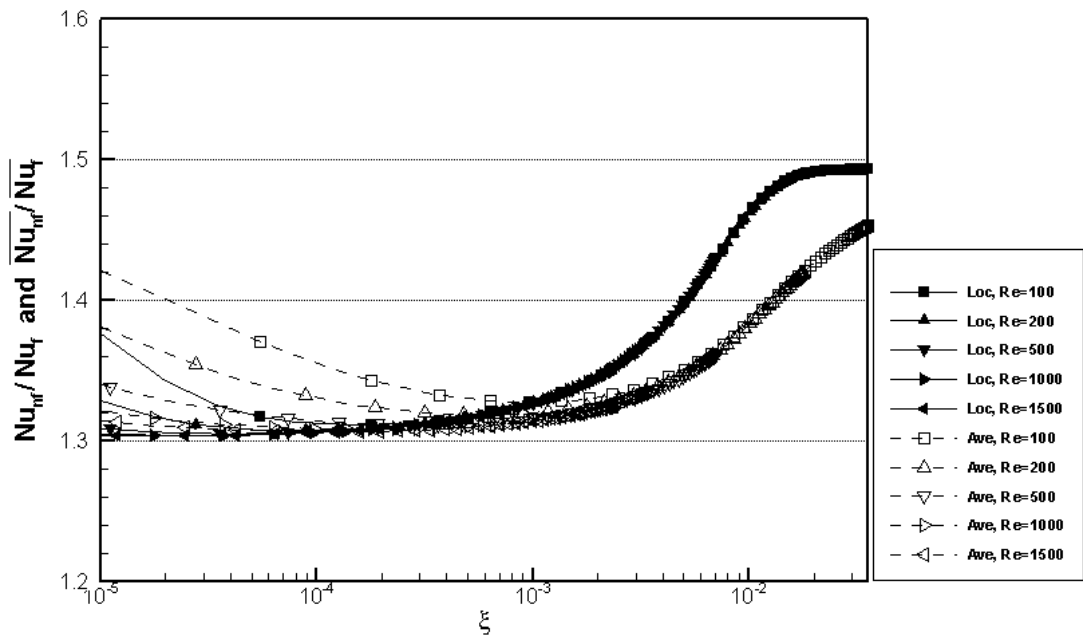
Figure 4.26: Local (Loc) and average (Ave) Nusselt number ratios, vs $\xi = \dfrac{x/D_e}{Re_{D_e}Pr}$ for parabolic entrance velocity and constant wall temperature for ϕ=5.0%

As seen in pictures, the ratio of local (Nu_{nf}/Nu_f) and average ($\overline{Nu_{nf}/Nu_f}$) Nusselt numbers increase as ξ increases, and after a specific value of ξ, it remains constant at about 1.49 for local and 1.45 for average ratios, for both cases of uniform and

parabolic entrance velocities. In the case of channel with parabolic entrance velocity scatter of data is seen at smaller ξ when Reynolds number is small.

4.4.3.2 Constant Wall Heat Flux

Local and average Nusselt numbers (based on T_b) with respect to ξ for pure fluid flow in channel with walls at constant heat flux are shown in Fig. 4.27 and Fig. 4.28, respectively for uniform and parabolic inlet velocities, for different values of Reynolds numbers.
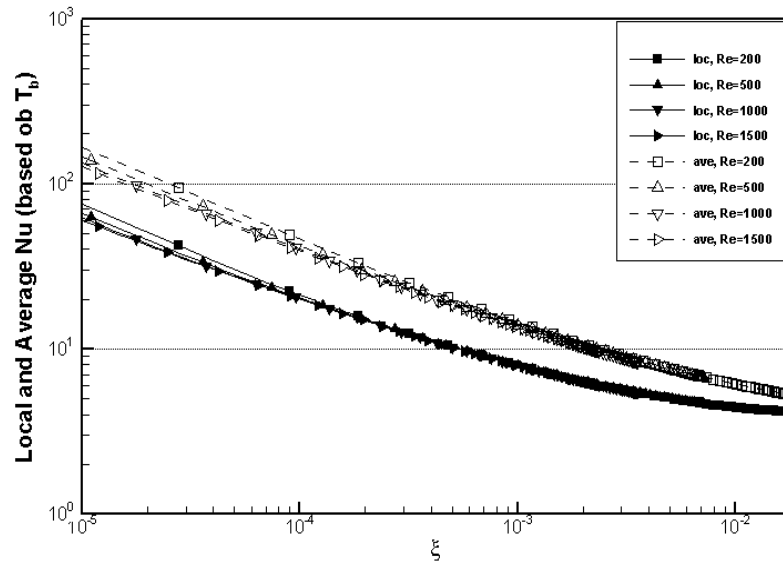
Figure 4.27: Local and average Nusselt number vs $\boldsymbol{\xi} = \dfrac{x/D_e}{Re_{D_e}Pr}$ for different Reynolds numbers, uniform entrance velocity for a pure fluid (ϕ=0.0%)
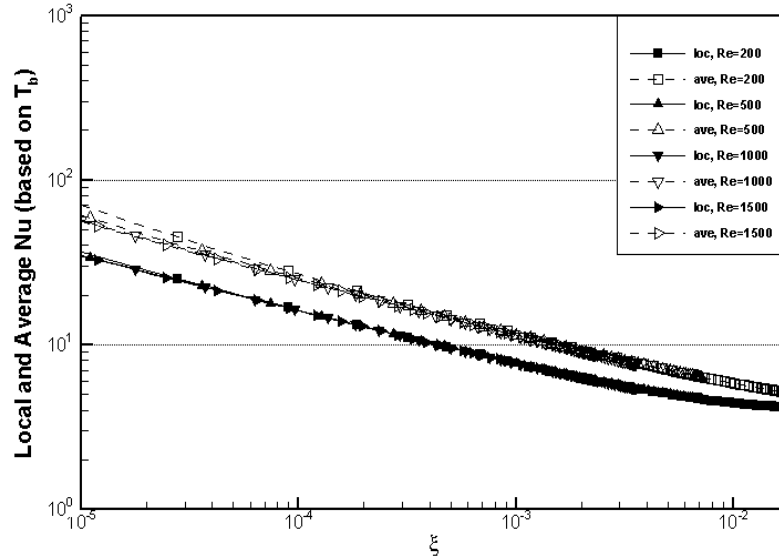
Figure 4.28: Local and average Nusselt number vs $\xi = \dfrac{x/D_e}{Re_{D_e}Pr}$ for different Reynolds numbers, parabolic entrance velocity for a pure fluid ($\phi=0.0\%$)

Similar to the case of walls at constant temperature, the local and average Nusselt numbers defined by Eq. 3.20 and 3.21 have to overlap for different values of Reynolds number, but as a result of numerical error as x approaches zero where Nusselt number approaches infinity, deviations are observed. For both uniform and parabolic entrance velocities the local and average Nusselt numbers converge to 4.1 ($Nu|_{\xi\to\infty} = \overline{Nu}|_{\xi\to\infty} = 4.1$).

In the following figures (Fig. 4.29 and Fig. 4.30) the local and average Nusselt numbers (based on T_b) have been compared for two cases of uniform and parabolic entrance velocities while walls are at constant heat flux.

Local Nusselt numbers (based on T_b) with respect to ξ for pure fluid flow in channel with walls at constant heat flux are shown in Fig. 4.29, for uniform and parabolic inlet velocities, for different values of Reynolds numbers.
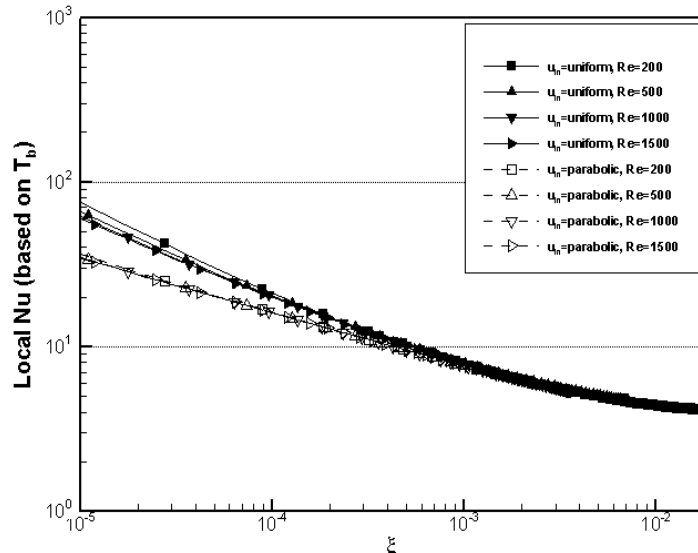
Figure 4.29: Local Nusselt number vs $\xi = \dfrac{x/D_e}{Re_{D_e}Pr}$ for uniform and parabolic entrance velocities and different Reynolds numbers for a pure fluid ($\phi=0.0\%$)

Local Nusselt numbers (based on T_b) with respect to ξ for pure fluid flow in channel with walls at constant heat flux are shown in Fig. 4.30, for uniform and parabolic inlet velocities, for different values of Reynolds numbers.
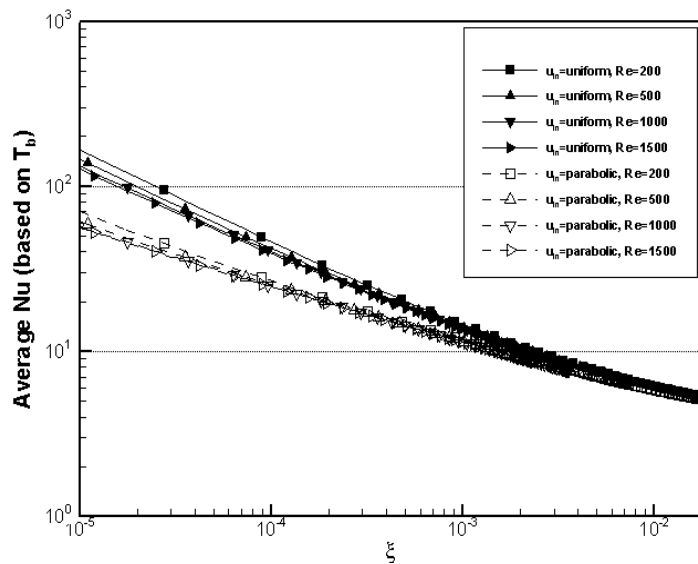
Figure 4.30: Average Nusselt number vs $\xi = \dfrac{x/D_e}{Re_{D_e}Pr}$ for uniform and parabolic entrance velocities and different Reynolds numbers for a pure fluid ($\phi=0.0\%$)

As seen in Fig. 4.29 and Fig. 4.30 the local and average Nusselt numbers are higher for channel with uniform entrance velocity compared to the channel with parabolic

59

entrance velocity at smaller values of ξ while for higher values of ξ, they converge to the same value (4.1).

Comparisons of local and average Nusselt numbers (based on T_b) between channels with walls at constant temperature, and constant heat flux are depicted in Fig 4.31 and Fig. 4.32 respectively for the case of uniform entrance velocity.
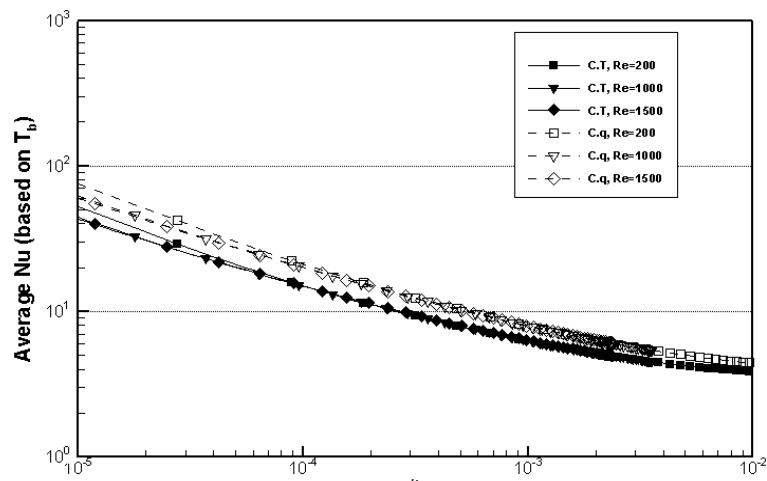
Figure 4.31: Local Nusselt number vs $\boldsymbol{\xi} = \dfrac{x/D_e}{Re_{D_e}Pr}$ for constant wall temperature (C.T) and constant wall heat flux (C.q), uniform entrance velocity and different Reynolds numbers for a pure fluid (ϕ=0.0%)
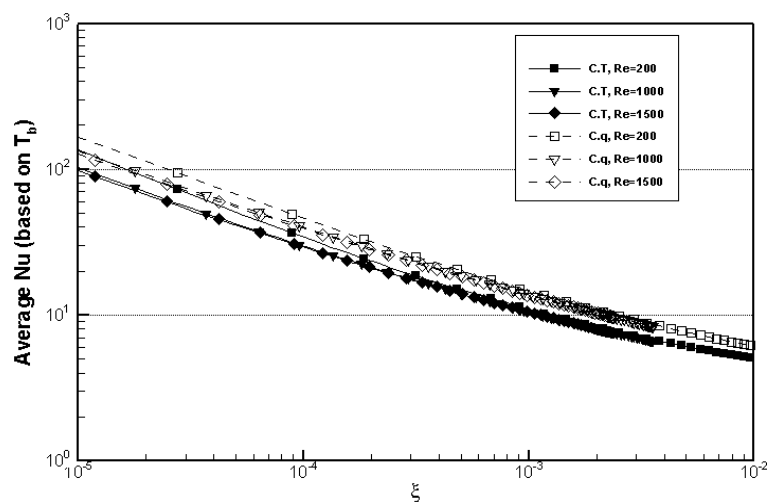
Figure 4.32: Average Nusselt number vs $\boldsymbol{\xi} = \dfrac{x/D_e}{Re_{D_e}Pr}$ for constant wall temperature (C.T) and constant wall heat flux (C.q), uniform entrance velocity and different Reynolds numbers for a pure fluid (ϕ=0.0%)

As shown in the figures both local and average Nusselt numbers are higher when walls are at constant heat flux compared to the channels with walls at constant temperature and as $\xi \to \infty$ local and average Nusselt numbers for the channel with walls at constant heat flux approach to 4.1 while for channel with walls at constant temperature they approach to 3.7.

The ratio of local (Nu_{nf}/Nu_f) and average ($\overline{Nu_{nf}}/\overline{Nu_f}$) Nusselt numbers (based on T_b) with 5% solid volume fraction nanofluid, are shown in Fig. 4.33 and Fig. 4.34 respectively for channel with uniform and parabolic inlet velocities, where walls are at constant heat flux.
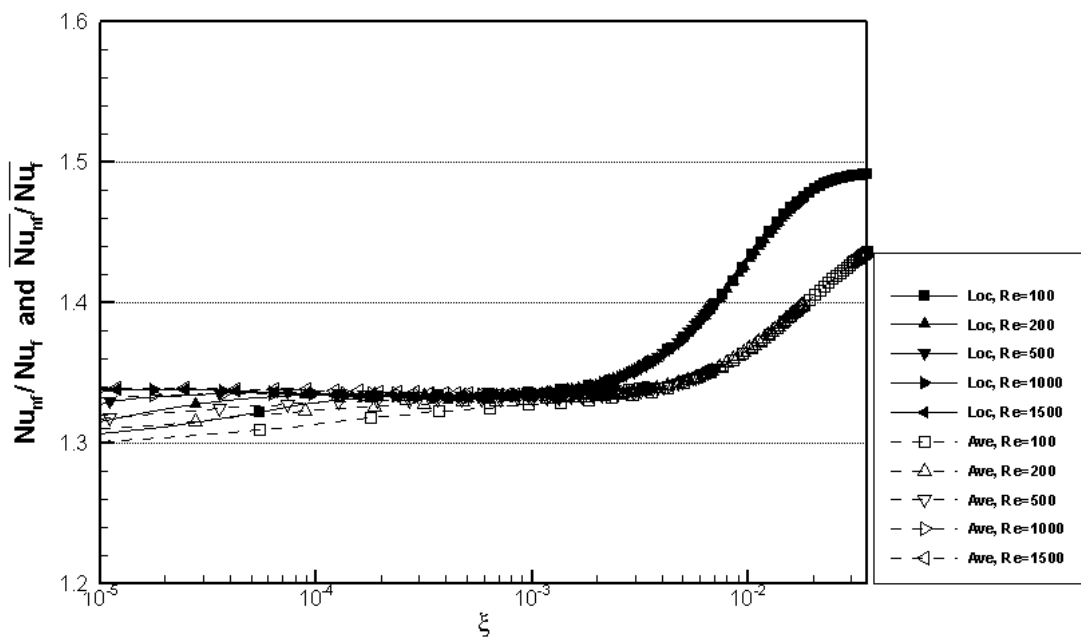
Figure 4.33: Local (Loc) and average (Ave) Nusselt number ratios, vs $\xi = \dfrac{x/D_e}{Re_{D_e}Pr}$ for uniform entrance velocity and constant wall heat flux for ϕ=5.0%
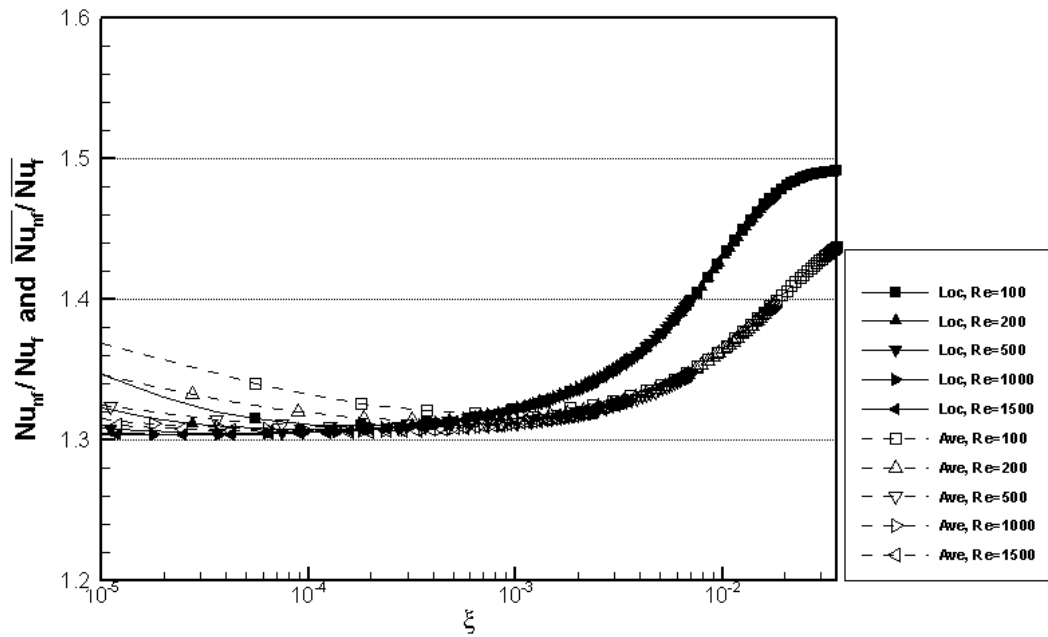
Figure 4.34: Local (Loc) and average (Ave) Nusselt number ratios, vs $\xi = \frac{x/D_e}{Re_{D_e}Pr}$ for parabolic entrance velocity and constant wall heat flux for ϕ=5.0%

As seen in pictures, the ratio of local (Nu_{nf}/Nu_f) and average ($\overline{Nu_{nf}}/\overline{Nu_f}$) Nusselt numbers increase as ξ increases, and after a specific value of ξ, it remains constant at about 1.49 for local and 1.43 for average ratios, for both cases of uniform and parabolic entrance velocities. In Fig. 4.34 for the channel with parabolic entrance velocity scatter of data is observed at small values of x when Reynolds number is small.

4.5 Investigation of Solid Volume Fraction, Reynolds Number, and Entrance Velocity Effects on Local and Average Shear Stresses

Considering that walls thermal boundary conditions do not have any effect on local and average shear stresses, the results for cases of walls with constant temperature and constant heat flux are exactly the same.

4.5.1 Local Wall Shear Stress

4.5.1.1 Uniform Entrance Velocity

The local wall shear stress is shown in Fig. 4.35 and Fig. 4.36 for uniform inlet velocity, with *Re*=100 and *Re*=1500 respectively, for different values of solid volume fractions.
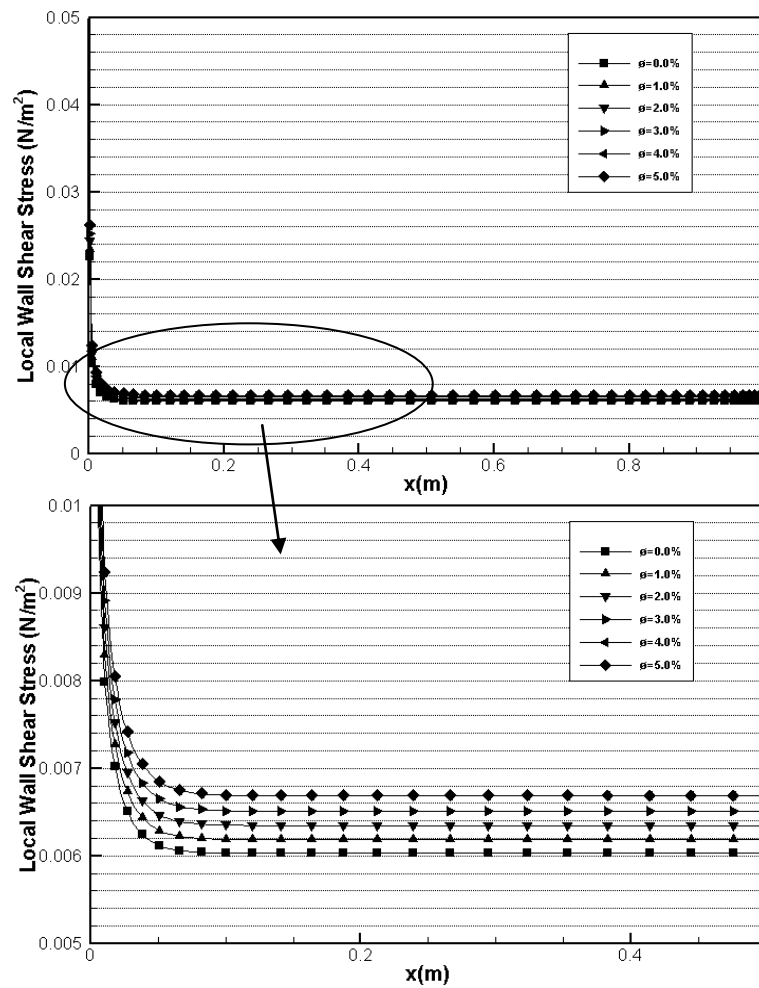
Figure 4.35: Variation of local wall shear stress with x for different solid volume fractions for uniform inlet velocity, *Re*=100.
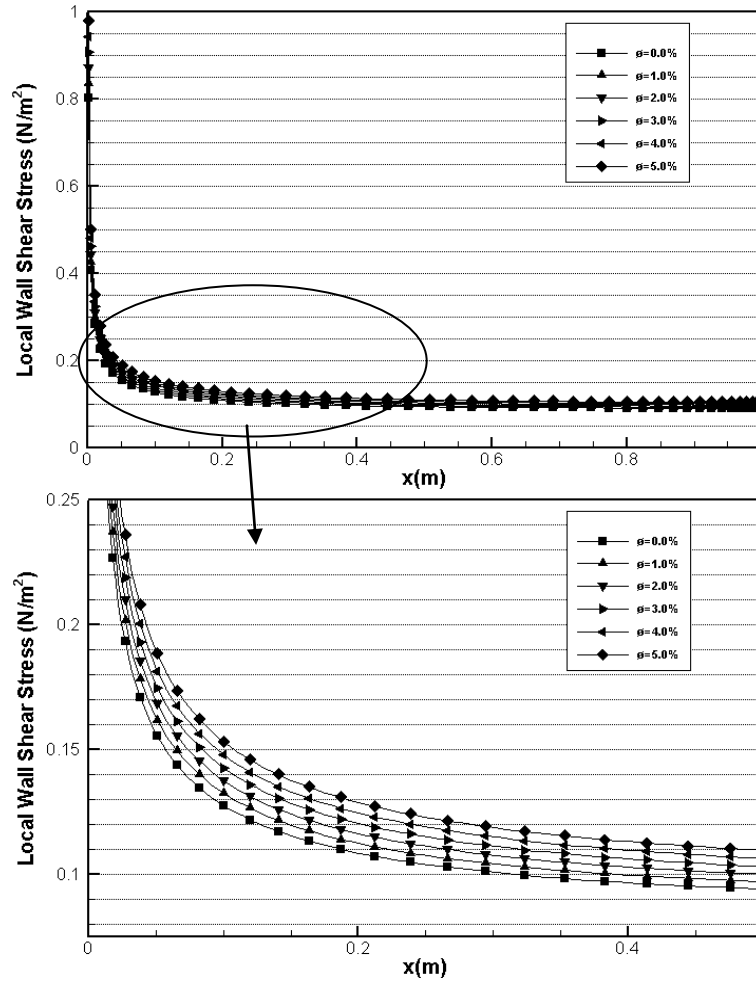
Figure 4.36: Variation of local wall friction factor with x for different solid volume fractions for uniform inlet velocity, *Re*=1500.

As indicated in Fig. 4.35 and Fig. 4.36 the local wall shear stress increases with ϕ at a constant Reynolds number. As solid volume fraction increases, the dynamic viscosity of nanofluid (μ_{nf}) increases, which results in an enhancement of τ_x (Eq. 3.22). Moreover the wall local shear stress decreases with x as velocity profile develops and remains constant when the flow is fully developed.

4.5.1.2 Parabolic Entrance Velocity

The local wall shear stress is shown in Fig. 4.37 and Fig. 4.38 for parabolic inlet velocity, with *Re*=100 and *Re*=1500 respectively, for different values of solid volume fractions.
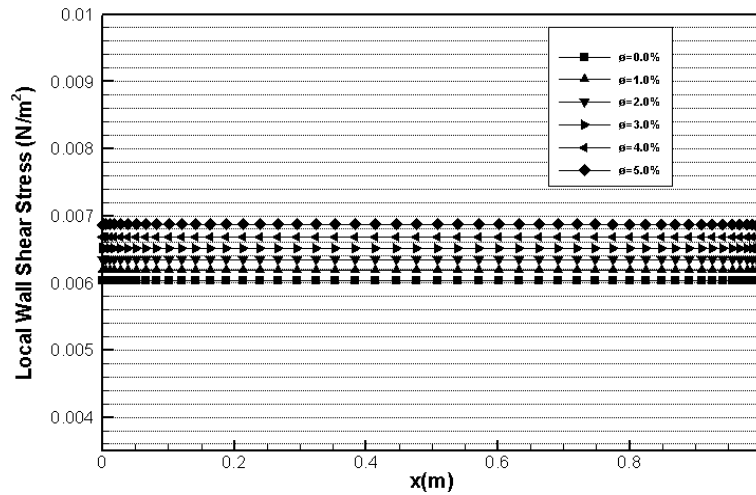
Figure 4.37: Variation of local wall shear stress with x for different solid volume fractions for parabolic inlet velocity, *Re*=100
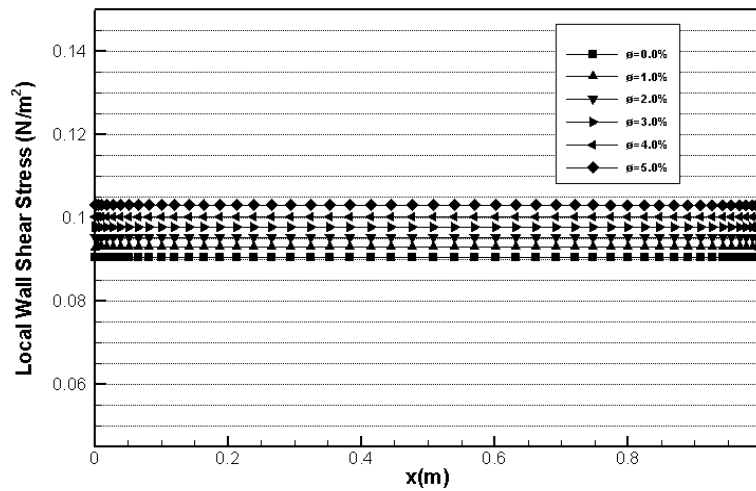
Figure 4.38: Variation of local wall shear stress with x for different solid volume fractions for parabolic inlet velocity, *Re*=1500

Similar to the uniform entrance velocity the local wall shear stress increases with solid volume fraction as the dynamic viscosity of nanofluid increases with ϕ at a constant Reynolds number. But unlike the last case the τ_x does not change with axial distance. Since the velocity profile is developed at the entrance it does not change with *x*, which keeps a constant $\frac{\partial u}{\partial y}$ along the *x* direction and results in a constant local shear stress at walls.

4.5.2 Average Wall Shear Stress

65

The variation of average wall shear stress with solid volume fraction (ϕ) for different *Re* is presented in Fig. 4.39 for the cases of uniform and parabolic entrance velocities, where the ratio of length to the width of channel is $\frac{L}{H} = 100$.
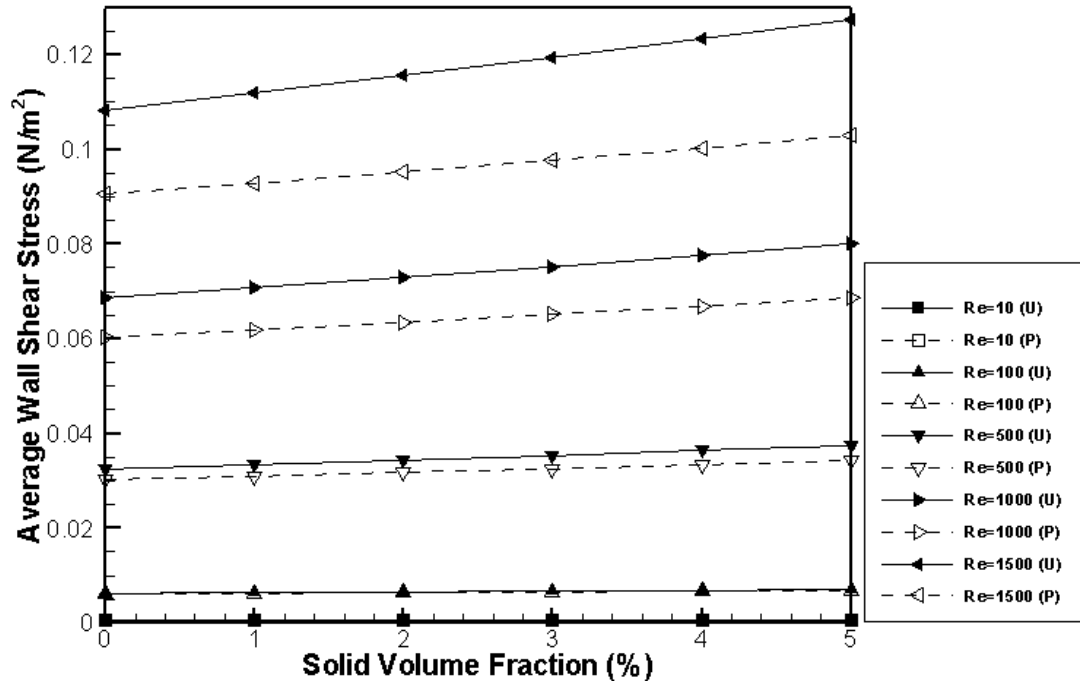
Figure 4.39: Average shear stress at walls for different *Re* and ϕ for uniform (U) and parabolic (P) entrance velocities

As illustrated in Fig. 4.39 average wall shear stress increases with increase in nanoparticle volume fraction for both cases. This happens as a result of nanofluid viscosity augmentation, with solid volume fraction. The augmentation of $\bar{\tau}$ at *Re*=10 is 13.7% when ϕ is increased from 0% to 5%, while this augmentation is 17.5% at *Re*=1500 (for channel with uniform entrance velocity). For parabolic entrance velocity $\bar{\tau}$ increases by 13.7% and 13.6% as ϕ increases from 0% to 5% for *Re*=10 and *Re*=1500, respectively. Likewise the average wall shear stress increases as *Re* increases.

In addition it can be seen that for a specific *Re* the average wall shear stress for channel with uniform entrance velocity is higher than channel with parabolic entrance velocity and this difference is bigger for larger values of *Re*. At *Re*=1500 for the pure fluid the $\bar{\tau}$ increases by 19.6% when the entrance velocity profile changes from parabolic to uniform.

Chapter 5

CONCLUSION

Hydrodynamic and thermal behavior of laminar flow in a rectangular duct has been studied with copper-water nanofluid coolant, considered as a Newtonian fluid. The range of the Reynolds numbers considered is between 10 and 1500, while solid volume fraction is considered to change between 0% and 5%. The diameter of nanoparticle is assumed to be 100 nm and thermophysical properties of the base fluid and the nanoparticle is considered to be constant at the inlet temperature. To determine the effective viscosity of nanofluid brinkman (Brinkman, 1952) model has been used while the model proposed by Patel et al. (Patel et al., 2005) has been utilized to find the effective thermal conductivity.

It has been observed that the rate of heat transfer increases with increase in solid volume fraction as well as with increase in Reynolds number. It is seen that the increase of heat transfer with solid volume fraction is bigger for higher Reynolds numbers. As presented in chapter 4, 5% increase in solid volume fraction results in augmentation of average wall Nusselt number by 30.3% for constant wall temperature and uniform entrance velocity, 29.6% for constant wall temperature and parabolic entrance velocity, 31.3% for constant wall heat flux and uniform entrance velocity, and 30.0% for constant wall heat flux and parabolic entrance velocity (when Re=1500).

Moreover higher heat transfer is observed for channel with uniform entrance velocity compared to channel with parabolic inlet velocity. For a pure fluid at Re=1500 and walls at constant temperature, the average Nusselt number increases by 4.4% when the entrance velocity profile changes from parabolic to uniform while this increment is 11.7% when walls are at constant heat flux.

The comparisons between two cases of constant wall temperature and constant wall heat flux indicate higher Nusselt number when walls are at constant heat flux. For the pure fluid at Re=1500 the average wall Nusselt number increases by 30.3% in the channel with uniform entrance velocity, when the thermal boundary conditions at the walls change from constant temperature to constant heat flux. This increase is 21.8% for a parabolic entrance velocity.

The average wall shear stress increases with solid volume fraction for channels with both uniform and parabolic entrance velocities. At Re=1500 as ϕ increases from 0% to 5% the average wall shear stress for the channel with uniform entrance velocity increases by 17.5%, while it increases by 13.6% for the channel with parabolic entrance velocity.

Also it can be indicated that the average wall shear stress is higher for the channel with uniform entrance velocity compared to channel with parabolic entrance velocity. For a pure fluid at Re=1500 the average wall shear stress increases by 19.6% when the entrance velocity profile changes from parabolic to uniform, while for a nanofluid with ϕ=5% this change is 5.2%.

REFERENCES

Alves, M. A., Oliveira, P. J., & Pinho, F. T. (2003). A convergent and universally bounded interpolation scheme for the treatment of advection. *International Journal for Numerical Methods in Fluids, 41*(1), 47-75. doi: 10.1002/fld.428

Brinkman, H. C. (1952). The Viscosity of Concentrated Suspensions and Solutions. *The Journal of Chemical Physics, 20*(4), 571-571

Bruggeman, Von Dag. (1935). Berechnung verschiedener physikalischer Konstanten von heterogenen Substanzen. I. Dielektrizitätskonstanten und Leitfähigkeiten der Mischkörper aus isotropen Substanzen. *Annalen der Physik, 416*(7), 636-664.

Choi, Stephen US, & Eastman, JA. (1995). Enhancing thermal conductivity of fluids with nanoparticles: Argonne National Lab., IL (United States).

Das, R., & Mohanty, A. K. (1983). Forced Convective Heat-Transfer in the Entrance Region of a Parallel Plate Channel. *International Journal of Heat and Mass Transfer, 26*(9), 1403-1405.

Das, Sarit Kumar, Choi, Stephen U. S., & Patel, Hrishikesh E. (2006). Heat transfer in Nanofluids - A review. *Heat Transfer Engineering, 27*(10), 3-19. doi: 10.1080/01457630600904593

Das, SK, Sundararajan, T, Pradeep, T, & Patel, HE. (2005). Physical Review Letters week ending. *Phys Rev Lett, 95*, 019402.

Einstein, Albert. (1956). *Investigations on the Theory of the Brownian Movement*: Courier Dover Publications.

Garnett, JC Maxwell. (1904). Colours in metal glasses and in metallic films. *Philosophical Transactions of the Royal Society of London. Series A, Containing Papers of a Mathematical or Physical Character*, 385-420.

Hamilton, RL, & Crosser, OK. (1962). Thermal conductivity of heterogeneous two-component systems. *Industrial & Engineering chemistry fundamentals, 1*(3), 187-191.

Heris, S. Zeinali, Esfahany, M. Nasr, & Etemad, S. Gh. (2007). Experimental investigation of convective heat transfer of Al2O3/water nanofluid in circular tube. *International Journal of Heat and Fluid Flow, 28*(2), 203-210. doi: 10.1016/j.ijheatfluidflow.2006.05.001

Hwang, Kyo Sik, Lee, Ji-Hwan, & Jang, Seok Pil. (2007). Buoyancy-driven heat transfer of water-based Al2O3 nanofluids in a rectangular cavity. *International Journal of Heat and Mass Transfer, 50*(19-20), 4003-4010. doi: 10.1016/j.ijheatmasstransfer.2007.01.037

Incropera, Frank P, Lavine, Adrienne S, & DeWitt, David P. (2011). *Fundamentals of heat and mass transfer*: John Wiley & Sons.

J.H. Lee, S.P. Jang. (2005). Fluid flow characteristics of Al2O3 nanoparticles suspended in water. *Trans. SAREK Winter Annual Conf, 22*, 546– 551.

Jang, S. P., & Choi, S. U. S. (2004). Role of Brownian motion in the enhanced thermal conductivity of nanofluids. *Applied Physics Letters, 84*(21), 4316-4318. doi: 10.1063/1.1756684

Jiji, Latif Menashi. (2006). *Heat convection*: Springer.

Kumar, D. H., Patel, H. E., Kumar, V. R. R., Sundararajan, T., Pradeep, T., & Das, S. K. (2004). Model for heat conduction in nanofluids. *Physical Review Letters, 93*(14). doi: 10.1103/PhysRevLett.93.144301

Maiga, S. E. B., Nguyen, C. T., Galanis, N., & Roy, G. (2004). Heat transfer behaviours of nanofluids in a uniformly heated tube. *Superlattices and Microstructures, 35*(3-6), 543-557. doi: 10.1016/j.spmi.2003.09.012

Patel, H. E., Sundararajan, T., Pradeep, T., Dasgupta, A., Dasgupta, N., & Das, S. K. (2005). A micro-convection model for thermal conductivity of nanofluids. *Pramana-Journal of Physics, 65*(5), 863-869. doi: 10.1007/bf02704086

Roy, G., Nguyen, C. T., & Lajoie, P. R. (2004). Numerical investigation of laminar flow and heat transfer in a radial flow cooling system with the use of nanofluids. *Superlattices and Microstructures, 35*(3-6), 497-511. doi: 10.1016/j.spmi.2003.09.011

Santra, Apurba Kumar, Sen, Swarnendu, & Chakraborty, Niladri. (2009). Study of heat transfer due to laminar flow of copper-water nanofluid through two isothermally heated parallel plates. *International Journal of Thermal Sciences, 48*(2), 391-400. doi: 10.1016/j.ijthermalsci.2008.10.004

Tzeng, S. C., Lin, C. W., & Huang, K. D. (2005). Heat transfer enhancement of nanofluids in rotary blade coupling of four-wheel-drive vehicles. *Acta Mechanica, 179*(1-2), 11-23. doi: 10.1007/s00707-005-0248-9

Wang, B. X., Zhou, L. P., & Peng, X. F. (2003). A fractal model for predicting the effective thermal conductivity of liquid with suspension of nanoparticles. *International Journal of Heat and Mass Transfer, 46*(14), 2665-2672. doi: 10.1016/s0017-9310(03)00016-4

Wang, Xinwei, Xu, Xianfan, & S. Choi, Stephen U. (1999). Thermal conductivity of nanoparticle-fluid mixture. *Journal of thermophysics and heat transfer, 13*(4), 474-480.

Wasp, Edward J, Kenny, John P, & Gandhi, Ramesh L. (1977). Solid--liquid flow: slurry pipeline transportation.[Pumps, valves, mechanical equipment, economics]. *Ser. Bulk Mater. Handl.;(United States), 1*(4).

Xuan, Y. M., & Li, Q. (2000). Heat transfer enhancement of nanofluids. *International Journal of Heat and Fluid Flow, 21*(1), 58-64. doi: 10.1016/s0142-727x(99)00067-3

Xuan, Y. M., & Li, Q. (2003). Investigation on convective heat transfer and flow features of nanofluids. *Journal of Heat Transfer-Transactions of the Asme, 125*(1), 151-155. doi: 10.1115/1.1532008

Xuan, Y. M., & Roetzel, W. (2000). Conceptions for heat transfer correlation of nanofluids. *International Journal of Heat and Mass Transfer, 43*(19), 3701-3707. doi: 10.1016/s0017-9310(99)00369-5

Yang, Y., Zhang, Z. G., Grulke, E. A., Anderson, W. B., & Wu, G. F. (2005). Heat transfer properties of nanoparticle-in-fluid dispersions (nanofluids) in larninar flow. *International Journal of Heat and Mass Transfer, 48*(6), 1107-1116. doi: 10.1016/j.ijheatmasstransfer.2004.09.038

Yu, B., Tao, W. Q., Wei, J. J., Kawaguchi, Y., Tagawa, T., & Ozoe, H. (2002). Discussion on momentum interpolation method for collocated grids of incompressible flow. *Numerical Heat Transfer Part B-Fundamentals, 42*(2), 141-166. doi: 10.1080/10407790190053879

Yu, W., & Choi, S. U. S. (2003). The role of interfacial layers in the enhanced thermal conductivity of nanofluids: A renovated Maxwell model. *Journal of Nanoparticle Research, 5*(1-2), 167-171. doi: 10.1023/a:1024438603801